SYNTHESIS AND CHARACTERIZATION OF NANOSTRUCTURES AND RAMAN MARKERS FOR BIO-DIAGNOSTICS USING SERS

A Thesis

submitted in partial fulfillment for the degree of

Master of Science

as part of the

Integrated PhD program

(Materials Science)

by

GAYATRI KUMARI

CHEMISTRY AND PHYSICS OF MATERIALS UNIT

JAWAHARLAL NEHRU CENTRE FOR ADVANCED SCIENTIFIC RESEARCH

BANGALORE – 560064, INDIA

APRIL 2011

DECLARATION

I hereby declare that the matter embodied in the thesis entitled **"Synthesis and Characterization of Nanostructures and Raman Markers for Bio-diagnostics using SERS"** is the result of investigations carried out by me at the Chemistry and Physics of Materials Unit, Jawaharlal Nehru Centre for Advanced Scientific Research, Bangalore, India under the supervision of Prof. Chandrabhas Narayana and it has not been submitted elsewhere for the award of any degree or diploma.

In keeping with the general practice in reporting scientific observations, due acknowledgment has been made whenever the work described is based on the findings of other investigators.

_____

Gayatri Kumari

CERTIFICATE

I hereby certify that the matter embodied in this thesis entitled **"Synthesis and Characterization of Nanostructures and Raman Markers for Bio-diagnostics using SERS"** has been carried out by Ms Gayatri Kumari at the Chemistry and Physics of Materials Unit, Jawaharlal Nehru Centre of Advanced Scientific Research, Bangalore, India under my supervision and that it has not been submitted elsewhere for the award of any degree or diploma.

_____

Prof. Chandrabhas Narayana
(Research Supervisor)

Acknowledgements

I would like to extend my sincere gratitude to my mentor and guide Prof. Chandrabhas Narayana who has been a constant source of inspiration for me. His guidance and support has enabled me to develop a detail understanding of the subject.

I would like to thank Prof. C. N. R. Rao, whose interest and love for science has been encouraging and stimulating for people like me.

I am thankful to the chairman of our unit, Prof. G.U. Kulkarni, for his guidance during the course work.

I would like to thank all the faculty members, especially Prof. Balasubramanian, Dr. Tapas Kumar Maji, Prof. Eswarmoorthy, Prof. Sunderesan, Prof. K.S. Narayan, Dr. T. Govindraju, Dr. Subi George, Dr. Ranjan Dutta, Prof. Ranganathan, Prof. Swapan K Pati, Prof. Shobhana Narasimhan, Dr. Vidhyadhiraja, Prof. Umesh Waghmare, Prof. S.M. Shivaprasad and Mrs. Shobha for the course work that proved to be very helpful during the course of research.

Discussions with Dr. Erode N. Prabhakaran regarding organic synthesis were very helpful and I would like to thank him for guiding me during that work. Scientific discussions with Dr. Uday Kumar Ranga regarding bio-molecule detection have been very useful. I would also like to thank Shravanthi, Aparna, Tirupathi and Damodar from organic chemistry lab at IISc for helping me in synthesis and Swaroopa from molecular virology lab here for helping me in working with biological samples.

I have found wonderful labmates in Dr. Gopal, Partha, Srinu, Soumik, Dhanya, Gayatri Nair,

Sharada, Dr. Santhosh and Dr. Deepti who have always been encouraging. I feel privileged to have such a wonderful group.

I would also like to thank my classmates Chidambar, Sharma, Rana, Arpan, Varun, Sudeshna, Dileep and Pandu with whom I have spent most of my time and who have made my stay here quite enjoyable.

I am here because of my college teachers especially Dr. Tandon, Dr. Sheikh and Dr. Roy who almost pushed me to pursue science as a career and I will always be grateful to them.

At last, I want to thank my parents and family members who were always a constant support behind me and appreciated me in all my endeavors.

Preface

Raman spectroscopy has made a tremendous progress in the last few years. With the advancement in technology, Raman spectrometers have become small, portable and do not require a trained person to handle it. Further, many developments have been made in the technique in order to carry out sensitive detection. The era has seen the discovery of techniques like Surface Enhanced Raman Scattering (SERS), Tip Enhanced Raman Scattering (TERS), Shell Isolated nanoparticles Enhanced Raman Scattering (SHINERS) and lab-on-chip detection technique involving microfluidic devices. This thesis mainly focuses on Surface Enhanced Raman Scattering. There are two mechanisms that are considered to be responsible for SERS: electromagnetic enhancement and chemical enhancement. Electromagnetic enhancement mechanism considers interaction of light with the metal nanoparticles while the latter comes into picture when a charge transfer complex is formed between the molecule and the nanoparticles giving rise to new energy states for electron excitation. Lately, detection by SERS has proved to be a very useful method as one can go up to single molecule detection. Major application of SERS is in the field of disease detection. Finding the concentration of contaminants in water, air, detection of toxicity level on food sample, detecting explosives are its other applications.

Chapter 1 presents an overview of Raman spectroscopy, SERS, SERRS and the theory behind these techniques. The second half of Chapter 1 gives a basic introduction to the following chapters. Chapter 2 gives the synthesis, characterization and SERS of benzotriazole derivatives and also talks about the effect of pH on SERS. Chapter 3 describes

the synthesis of three layer core shell nanostructure Ag@SiO_2@Au and its use as a SERS substrate. In second part of this chapter, importance of capping agent on nanoparticles and its role in SERS has been shown. Chapter 4 talks about bio detection using SERS, wherein the synthesis and characterization of magnetic core shell nanoparticles have been discussed and how DNA detection can be done by adopting a three way detection process.

Table of Contents

Abbreviations

APTES: 3-aminopropyl triethoxysilane

Bz: Benzene

BTA: Benzotriazole

BTAA: 1H 1,2,3-benzotriazol 1-yl acetic acid

CTAB: N,N,N,N,-Cetyl trimethyl ammonium bromide

CV: Crystal Violet

Cy 5: Cyanine 5

EBTA: Ethyl 1H 1,2,3-benzotriazol 1-yl acetate

Na. Citr.: Trisodium citrate

np: nanoparticle

PCR: Polymerase chain reaction

PDC: 1,4 Phenylene diisothiocyanate

PVP: Polyvinyl pyrrolidone

R6G: Rhodamine 6G

RB: Round bottom flask

ssDNA: single stranded DNA

SPR: Surface plasmon resonance

TEOS: Tetraethyl orthosilicate

THPC: Tetrakis hydroxymethyl phosphonium chloride

Tz: Triazole

Chapter 1

Introduction

The foundation of scattering phenomena of light was laid as early as 1922 when Brillouin predicted scattering of light by long wavelength elastic sound waves [1]. Later in 1928, Sir C. V. Raman and K. S. Krishnan discovered the Raman Effect [2], which describes the inelastic scattering of light by molecules. Soon it was realized that this phenomenon is an excellent tool to study excitations of molecule and get information about molecular structure. Raman scattering is a weak process (one part in a million photons get scattered inelastically) and use of mercury lamps then (not a very good light source) further disregarded its use as a fundamental tool. The discovery of laser and intense monochromatic sources in 1960 saw progress in light scattering and the beginning of a new era. Since then there has been rapid expansion in the versatility of Raman system that now incorporates microscopes and fiber optic bundles to illuminate and view the sample. Thus, with the development in technology Raman scattering has emerged out as very important technique for molecule characterization.

Last few decades have witnessed the growing use of Raman scattering in various fields. The advantage of using this technique lies in the fact that this technique needs no sample preparation. Raman scattering measurements can be done in any state of sample like solid, liquid or gaseous, and is also independent of sample size. But, there is a drawback

associated with Raman scattering, i.e., only one part in a million of total intensity of the incident light is Raman scattered. This drawback was overcome with Resonance Raman spectroscopy and with the discovery of Surface Enhanced Raman Scattering (1974), wherein the signal intensity is enhanced by the use of roughened metal surfaces or metal nanoparticles. Fleischmann et al. [3] in 1974 observed intense Raman scattering from pyridine adsorbed onto roughened silver electrode surface from aqueous solution. Later, Jeanmarie and Van Duyne [4] proposed electric field enhancement mechanism for SERS. SERS is even more powerful when the laser frequency is resonant with the frequency of electronic transitions of molecule and this phenomenon is known as Surface Enhanced Resonant Raman Scattering (SERRS). Both SERS and SERRS are extensively used for bio detection and ultra trace analysis. In this chapter we briefly discuss Raman scattering and all phenomena related to it giving an overview of mechanisms happening in different light scattering processes.

1.1 Raman Scattering

There are several ways in which light can interact with matter: it can be absorbed, scattered or transmitted. When a light wave (an oscillating dipole) passes through a molecule, it can polarize the electrons and excite it to a high energy state called virtual state. In this state, the energy transfer from the light to the molecule can take place through the formation of very short lived complex between light and electrons. This complex being unstable releases light in the form of scattered radiation. The actual shape

of the distorted electronic arrangement will depend on how much energy is transferred to the molecule and is dependent on the energy of the laser used. Hence laser frequency is one of the defining factors for the energy of the virtual state and the extent of distortion.

Let us consider an electromagnetic wave with the electric field [5]

$$E = E_O \cos\left(2\pi\nu_O t\right) \qquad \ldots(1)$$

interacting with the molecule. Then this electric field will induce dipole in the molecule, given by

$$\vec{P} = \tilde{\alpha}.\vec{E} \qquad \ldots(2)$$

where $\tilde{\alpha}$ is the polarizability tensor which varies with time and its components can be represented as elements of matrix

$$\begin{bmatrix} p_x \\ p_y \\ p_z \end{bmatrix} = \begin{bmatrix} \alpha_{xx} & \alpha_{xy} & \alpha_{xz} \\ \alpha_{yx} & \alpha_{yy} & \alpha_{yz} \\ \alpha_{zx} & \alpha_{zy} & \alpha_{zz} \end{bmatrix} \begin{bmatrix} E_X \\ E_Y \\ E_Z \end{bmatrix} . \qquad \ldots (3)$$

α gives the response of electron distribution to the movement of nuclei that oscillate with the normal mode frequency ν_m. Thus $\tilde{\alpha}$ can be expressed as

$$\tilde{\alpha} = \tilde{\alpha}_O + \left(\frac{\partial\tilde{\alpha}}{\partial q}\right)_O q_O \cos\left(2\pi\nu_m t\right) + \ldots \qquad \ldots(4)$$

From Equations (2) and (4), we have

$$\begin{aligned}\vec{P} &= \tilde{\alpha}\vec{E}_O \cos(2\pi\nu_O t) \\ &= \alpha_O \vec{E}_O \cos(2\pi\nu_O t) + \\ &\frac{1}{2}\left(\frac{\partial\tilde{\alpha}}{\partial q}\right)_O q_O \vec{E}_O \left[\cos\{2\pi(\nu_O + \nu_m)t\} + \cos\{2\pi(\nu_O - \nu_m)t\}\right]\end{aligned}$$

…(5)

Right side of Eq. (5) has three terms. The first term corresponds to *Rayleigh scattering* (elastic scattering) where the scattered frequency is same as the frequency of incident light, whereas the other two terms correspond to inelastic scattering (frequency shifted) known as *Raman scattering*. When the frequency of the scattered light is lower than v_o, it is *Stokes scattering* while when it is higher it is *anti-Stokes* scattering as shown in figure 1.1.

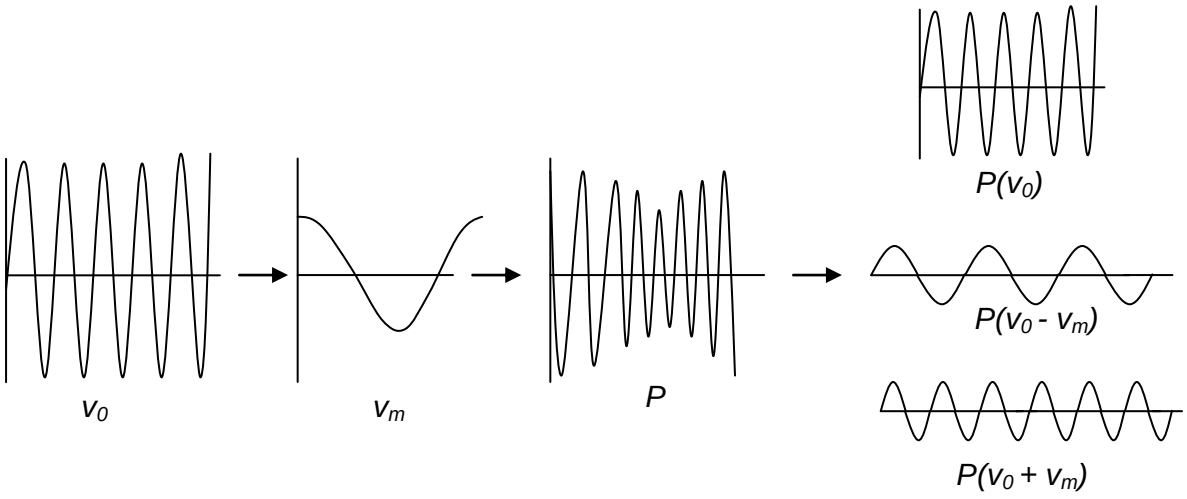

Figure 1.1: Time dependence of linear induced dipoles produced by electromagnetic radiation of frequency v_o [6].

Classical mechanics alone cannot completely explain Raman scattering. It needs quantum mechanical treatment which describes the interaction of vibrational quantum states with electromagnetic radiation. These states are defined by a set of quantum numbers and a corresponding wave function. There are ground and excited electronic

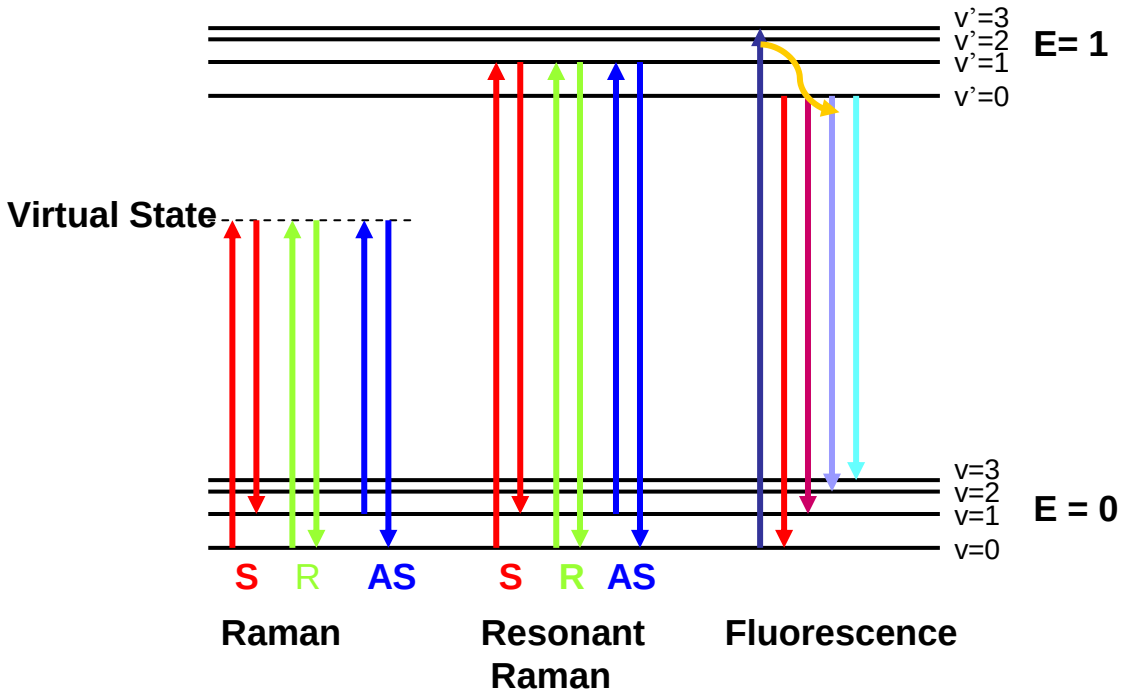

Figure 1.2: Energy level diagram to show the Raman, Resonant Raman and fluorescence processes.

states each having vibrational energy states. In Rayleigh or Raman scattering, transition takes place via virtual state (an imaginary state) in which one photon is absorbed and another photon of same energy (Rayleigh scattering) or of lower energy (stokes lines) or

of higher energy (anti stokes lines) is emitted. Figure 1.2 shows this process. The virtual state shown here does not correspond to any eigen state of the system and hence is an unreal state. The time of stay of electrons in these states are very small, that is of the order of femtoseconds.

The intensity of the emitted radiation, apart from depending on the intensity of incoming radiation, also depends on the Raman cross section. For the transition from vibrational state n to m,

$$I_{n\to m} = \sigma_{n\to m} I_o \qquad \ldots (6)$$

where $\sigma_{n\to m}$ is the Raman scattering cross section, I_o is the intensity of the incident radiation, $I_{n\to m}$ is the intensity of scattered radiation integrated over all scattering angles and polarization direction for a non oriented sample. The Raman cross section is related to Raman polarizability [5] by

$$\sigma_{n\to m} \propto (\nu_o \pm \nu_m)^4 . \sum_{p,\sigma} \left| \alpha_{p,\sigma} \right|^2 \qquad \ldots (7)$$

taking into consideration that the intensity of electric dipole radiation scales as fourth power of frequency. The indices p and σ denote the molecule fixed co-ordinates.

On the basis of Kramers-Heisenberg-Dirac's dispersion theory, scattering tensor can be expressed as

$$[\alpha_{nm}]_{\rho\sigma} = \frac{1}{h}\sum_{R,r}\left(\frac{\langle nG|M_p|Rr\rangle\langle rR|M_\sigma|Gm\rangle}{\nu_{Rr}-\nu_m-\nu_o+i\tau_R}\right)+\left(\frac{\langle Rr|M_\sigma|Gm\rangle\langle nG|M_\rho|Rr\rangle}{\nu_{Rr}-\nu_m+\nu_o+i\tau_R}\right)$$

…(8)

where M_σ (M_ρ) is the electronic transition dipole given in terms of molecule fixed co-ordinate σ and ρ [7,8]. Indices R and r refer to the electronic and vibrational states of the molecule respectively, τ_R is damping constant and depends on the lifetime of the vibronic state Rr. Equation (8) represents the transition between nG to Gm via Rr. The sum indicates that for any Raman transition, all vibronic states have to be considered and Raman intensities as well as scattering tensor is controlled by transition probabilities involving all vibronic states, even though the initial and final states refer to the vibrational ground and excited states of the electronic ground state.

Another important point to be discussed here is the selection rule for Raman scattering. A molecule with N number of atoms will have 3N degrees of freedom. Three of these degrees of freedom describe the translational motion of molecule in space while another three (two for linear molecule) describe rotational motion. Thus, a non- linear molecule will have 3N-6 vibrational degrees of freedom or possible vibrations while a linear molecule will have 3N-5 possible vibrations. But, not all these modes of vibrations are seen in Raman spectra. For a particular mode of vibration to be observed in Raman or to be Raman active, there should be a change in polarizability of the molecule. In above

equations we saw that both, dipole moment *p* and polarizability α vary linearly in x, that is they are said to vary harmonically with x. However, if higher order terms of x are also included, this will bring in the anharmonicity. This anharmonicity will cause the vibrational selection rule $\Delta v = \pm 1$ to be modified to $\Delta v = \pm 1, \pm 2, \pm 3$ and so on. But these overtone transitions $\Delta v = \pm 2, \pm 3\ldots$ are usually weak compared to the transitions $\Delta v = \pm 1$. Few general selection rules for Raman intensity as given by Andreas C. Albrecht [7] have been summarised below,

1. " *A given pair of pure electronic states cannot contribute to Raman intensity if a dipole transition to either or both is purely forbidden.*"

2. " *A pair of configurations which differ in molecular orbital occupancy by more than one electron cannot mix (under vibrational perturbation) and as a pair cannot contribute to Raman intensity .* "

1.1.1 Resonance Raman scattering

Resonance Raman scattering occurs when the frequency of laser beam, ν_o happens to be close to the frequency of electronic transition. Hence, here both the ground state and the excited states are real states. Eqn (8) for resonance Raman can be simplified to

$$\left[\alpha_{nm}\right]_{\rho\sigma} \cong \frac{1}{h}\sum_{r}\left(\frac{\left\langle nG\left|M_{\rho}\right|Rr\right\rangle\left\langle rR\left|M_{\sigma}\right|Gm\right\rangle}{\upsilon_{Rr}-\upsilon_{m}-\upsilon_{o}+i\tau_{R}}\right). \qquad \ldots(9)$$

Here the denominator reduces to a small value, and scattering cross section of the

molecule is increased by several folds. Hence, the signal intensity becomes very high when the resonance Raman condition is satisfied. Again, here one can see several Raman lines that are shifted from the excitation line by vibrational quanta differing by one. They correspond to transitions to higher vibrational levels of ground electronic state. Resonant Raman can be observed in molecules with chromophores like Rhodamine 6G, Cy5 (cyanine dyes) etc.

1.2 Surface Enhanced Raman Scattering (SERS)

Surface enhanced Raman scattering was discovered by Fleischmann *et al.* [3] in 1974 and later recognized independently by two groups namely; Jeanmarie and Van Duyne [4] and Albrecht and Creighton [9]. As the name suggests, SERS is the enhancement of Raman signal due to the presence of roughened metal surface (roughness in the scale of nanometer, quite easily observed in the case of metal nanoparticles) in the vicinity of molecules. The Raman signal is enhanced by factor of 10^6 to 10^8 times. Due to high enhancement factor, SERS has been one of the important tools for trace analysis of molecules and for biodetection. As an example, these have been introduced in the high denomination Euro notes as security measures. There are two mechanisms considered responsible for SERS: Electromagnetic Enhancement and Chemical Enhancement [10] .

1.2.1 Electromagnetic Enhancement

Collective oscillations of surface free electrons of a conductor are known as *Surface Plasmons*. When the size of the particles or the surface roughness features are smaller

than the wavelength of incident light, then the electromagnetic field of light can effectively couple with these surface plasmons, inducing an electric dipole moment in the nanoparticles. The incident field excites the surface plasmon causing an additional electric field component normal to the surface near the sphere. Thus, the field in the vicinity of the molecule is the sum of the incident field and the induced field.

Let us consider a metal nanoparticle of radius r and complex dielectric constant ε(ν). Let there be a molecule at a distance d from this nanoparticle experiencing a field E_M which is the sum of the incident field and the induced field. The field enhancement factor A(ν) is the ratio of the field felt by the molecule and the incoming field, and is given by

$$A(\nu) = \frac{E_M(\nu)}{E(\nu)} = \frac{\varepsilon - \varepsilon_o}{\varepsilon + 2\varepsilon_o}\left(\frac{r}{r+d}\right)^3 \qquad \ldots(10)$$

The value of enhancement factor is large when Re (ε) = $-2\varepsilon_o$ and the imaginary part of dielectric constant is small. Metals like Cu, Ag and Au satisfy this resonance condition at visible wavelengths and hence exhibit strong SERS. Taking into account, the enhancement due to laser field and the stokes field, the enhancement factor for stokes scattering is given by

$$G(\nu_s) = \left|A(\nu_L)\right|^2 \left|A(\nu_S)\right|^2 = \left|\frac{\varepsilon(\nu_L) - \varepsilon_o}{\varepsilon(\nu_L) + 2\varepsilon_o}\right|^2 \left|\frac{\varepsilon(\nu_S) - \varepsilon_o}{\varepsilon(\nu_S) + 2\varepsilon_o}\right|^2 \left(\frac{r}{r+d}\right)^{12}$$

$\ldots(11)$

It can be seen from the above equation that the enhancement factor scales as fourth power of the local field at the vicinity of molecule. Secondly, electromagnetic enhancement decays with distance as $(r/(r+d))^{12}$. Electromagnetic enhancement accounts for enhancement of about 10^4 to 10^6 [11,12].

1.2.2 Chemical Enhancement

Chemical enhancement is basically due to the formation of adsorbate-surface complex leading to charge transfer phenomena either from metal to molecule or vice versa. It is attributed to chemisorption interaction, photon driven charge transfer between adsorbate and substrate, and coupling effect between the electron hole-pair and adsorbed molecules. Though the process results in weak enhancement, they are responsible for frequency shifts and relative intensity of spectral bands [13]. Figure 1.3 shows the HOMO and LUMO of the adsorbate (molecule), the Fermi level of the metal and the charge transfer directions. Molecules mostly studied by SERS typically have their lowest lying electronic excitations in the near ultraviolet region which would put the charge transfer excitations in the visible region of spectrum [10]. Chemical enhancement accounts for enhancement of about 10-100 in magnitude.

In addition to the above mentioned phenomena, there is another phenomenon which results in the increase in enhancement factor. This is known as Surface Enhanced Resonance Raman Scattering (SERRS). It occurs when the laser frequency is tuned to the excitation frequency of fluorescent molecules adsorbed on roughened metal surfaces or

metallic nanoparticles. This leads to large enhancements (10^7 to 10^{14}) in the Raman signal of molecule.

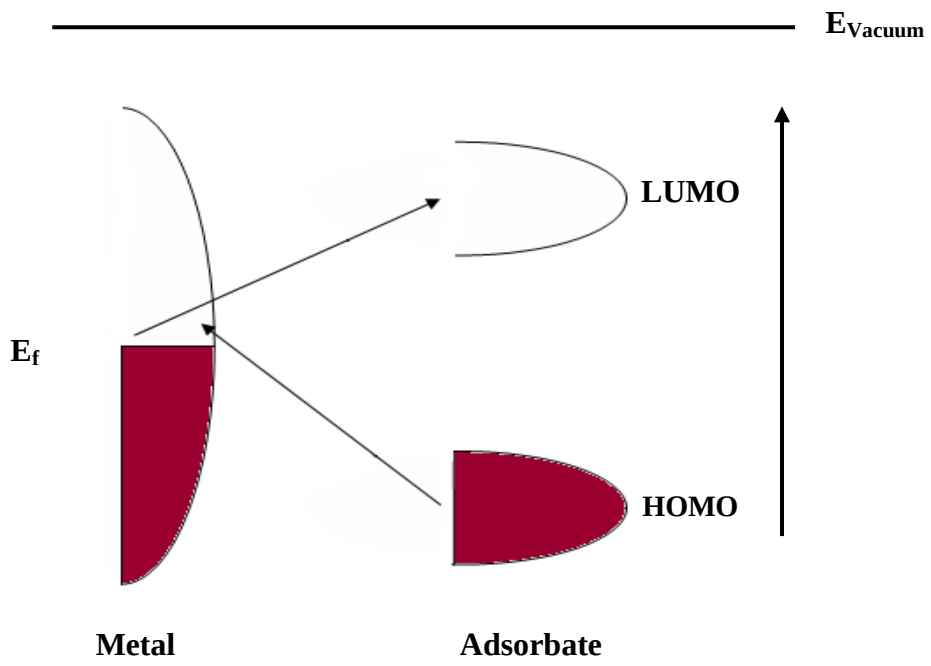

Figure 1.3: Energy level diagram for a molecule adsorbed on metal surface. Possible charge transfer excitations are shown [10].

1.2.3 Calculation of SERS Enhancement Factor

SERS Enhancement factor can be calculated in the following way [14,15].

1. First the Raman spectra of a molecule of a given concentration C_R, is recorded.

2. Raman integral intensity I_R, of one of the strong bands is calculated.

3. SERS spectra of same molecule at some lower concentration C_S, is recorded.

4. SERS integral intensity I_S, of the same band is calculated.

Then SERS Enhancement factor G is given by,

$$G = \frac{C_R}{C_S} \times \frac{I_S}{I_R} \ . \qquad \ldots (11)$$

It should be noted that laser power, accumulation time, scattering geometry etc has to be same for Raman and SERS measurements. In the following sections it will be discussed as to how to modify the inherent characteristics of molecule and nanoparticles so as to achieve high enhancement factor for SERS.

1.3 SERS Markers

SERS markers can be thought of as composite system of metal nanoparticles and molecules that are Raman active. Metal nanoparticles increase the electric field in its vicinity and also provide intermediate states for electron transfer from, or to the molecule. By changing the shape and the size of nanoparticles we can obtain very high fields at the molecule coupled with charge transfer process discussed in earlier section. Nanoparticles and their SERS will be discussed in detail in the next section, here the main attention will be on the molecules and dyes that are Raman active. All molecules have vibrations associated with them and have some signature in Raman spectrum but all molecules cannot be used as Raman or SERS markers. This is because the intensity of the peaks obtained in Raman is very weak due to the selection rules. Moreover, scattering cross section is also small for small and non-conjugated linear molecules. Raman or SERS active molecules are molecules mostly with benzene rings and exhibit absorption in the visible region. These molecules have a signature Raman spectrum. Common

Raman active molecules used for SERS are Rhodamine dyes (Rhodamine 6 G, Rhodamine B), Cyanine dyes (Cy 5, Cy 3.3), cystal violet etc. But these molecules are highly fluorescent in nature so that their Raman spectrum has a large fluorescence background and the Raman peaks get masked due to this.

Further, the aim here is to use them for DNA detection process. So, it is required that these dyes must have end groups that can be easily functionalised to attach to the oligonucletide, but this is a bit rigorous reaction. Therefore a molecular system should be designed to overcome these problems. To do this new molecules that act as Raman markers and are easily attachable to oligonucletides are synthesized. The molecule of interest is benzotriazole. This molecule and its derivatives are known to act as corrosion inhibitors for copper and copper based alloys in various corrosive environments [16]. The corrosive action is due to formation of protective film of copper triazole polymeric complex at high pH and high potentials whereas it gets adsorbed on copper surface at low pH and less noble potentials [17] . Hence the molecule shows different behaviour at different pH. Additionally, this molecule can easily undergo substitution reaction at 1-N and hence can be modified as per our needs.

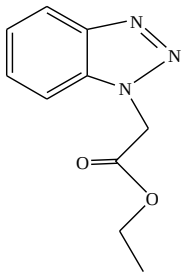

A) Ethyl 1H 1,2,3-benzotriazol 1-yl acetate

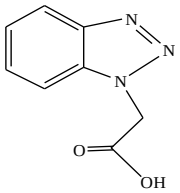

B) 1H 1,2,3-benzotriazol 1-yl acetic acid

We have synthesized two different benzotriazole derivatives whose structure have been shown above, the acetic acid and the ester derivative. These molecules give good Raman signals. Further, SERS of the acid derivative varies significantly with pH. It binds through the nitrogen of triazole group at acidic pH and the strong peaks observed in SERS are mainly of the triazole group. Secondly, the binding is through oxygen of carboxyl group at basic pH and here again the carboxyl stretching frequency and benzene ring frequency have stronger signatures while triazole peaks are very weak. So, with the change in pH conditions, the orientation of the molecule at the surface of the nanoparticles changes and thus the group which are nearer to the nanoparticle are more enhanced compared to the others. This property makes it suitable for its application in DNA detection at variable pH conditions. Benzotriazole can be covalently attached to the oligonuceotides by a linker molecule mediated by spacer methylene groups. The other end of the oligonucleotide can be modified to bear a COOH group and the two near ends sequences can be made such that they are complementary to each other. So in absence of any complementary oligonucletide sequence, the capture probe forms a stem loop kind of structure keeping the carboxyl end and the benzotriazole moiety together. It can be speculated that this structure would facilitate SERS to be observed almost at entire pH range. Now as the molecule hybridizes with the target sequence the loop opens increasing the distance between the benzotriazole group and the COOH group. For this configuration it can be said that SERS signal will be obtained at acidic pH when the

molecule orients itself so that the binding takes place through the triazole group. If the binding happens through COOH group (that is at basic pH), SERS signal would change confirming that the binding has taken place. So the change can be used to detect the presence of target oligonucletide.

Another advantage of using benzotriazole derivative molecules is that these molecules are less fluorescent than the conventionally used Raman active dyes. Chapter 2 describes the synthesis of these molecules, their characterization and the pH dependent SERS studies.

1.4 Nanostructures

When a small metal nanoparticle is kept in an oscillating electric field, the conduction electrons of the nanoparticles also start oscillating coherently as shown in the figure 1.4 [18].

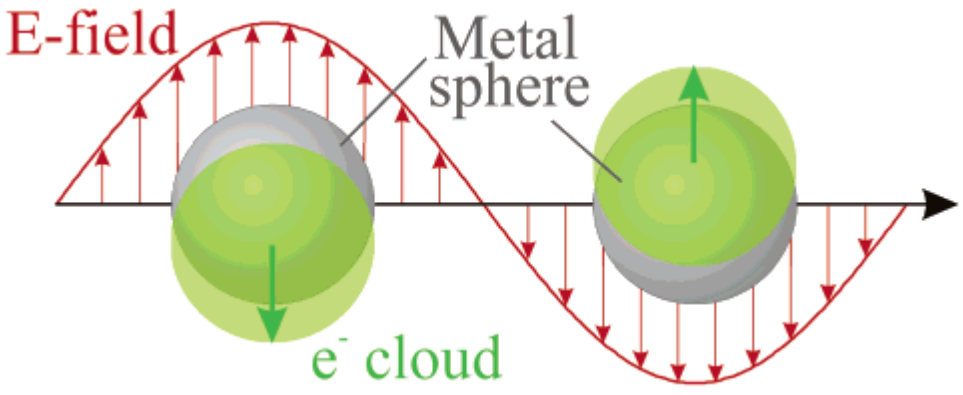

Figure 1.4: Plasmon oscillation of a metallic sphere showing the displacement of conduction electron relative to nuclei .

A restoring force arises due to the coulombic interaction between the electron and nuclei resulting in oscillation of electron cloud, relative to the nucleus. Four factors govern the oscillation frequency: the density of electron, the effective electron mass, the shape and the size of charge distribution. This collective oscillation of conduction electron in the presence of an oscillating field is called dipole plasmon resonance of the particle. Higher modes like quadruple mode of plasmon excitation can occur wherein half the electron cloud moves parallel to field while the other half moves antiparallel. For metals like silver, plasmon frequency is also affected by the electrons present in the d-orbital. Figure 1.5A shows the real and imaginary part of silver metal dielectric constant as a function of wavelength. The second and third plot, 1.5B and 1.5C show the extinction efficiency, i.e., the ratio of extinction cross section to the geometrical area as a function of wavelengths for silver sphere of 30 nm and 60 nm respectively. The plots show the results obtained from both quasistatic theory and Mie theory [18].

As discussed before, plasmon resonances of nanoparticles strongly depend on their composition, shape and size [19-22]. The resonant excitation of plasmons can amplify the electric field in the near vicinity of nanoparticles and so these nanoparticles play a key role in SERS**.** By changing the shape of nanoparticles, its surface plasmon resonance can be tuned to match the laser frequency as well as the absorption wavelength of the molecule and hence obtain maximum enhancement.

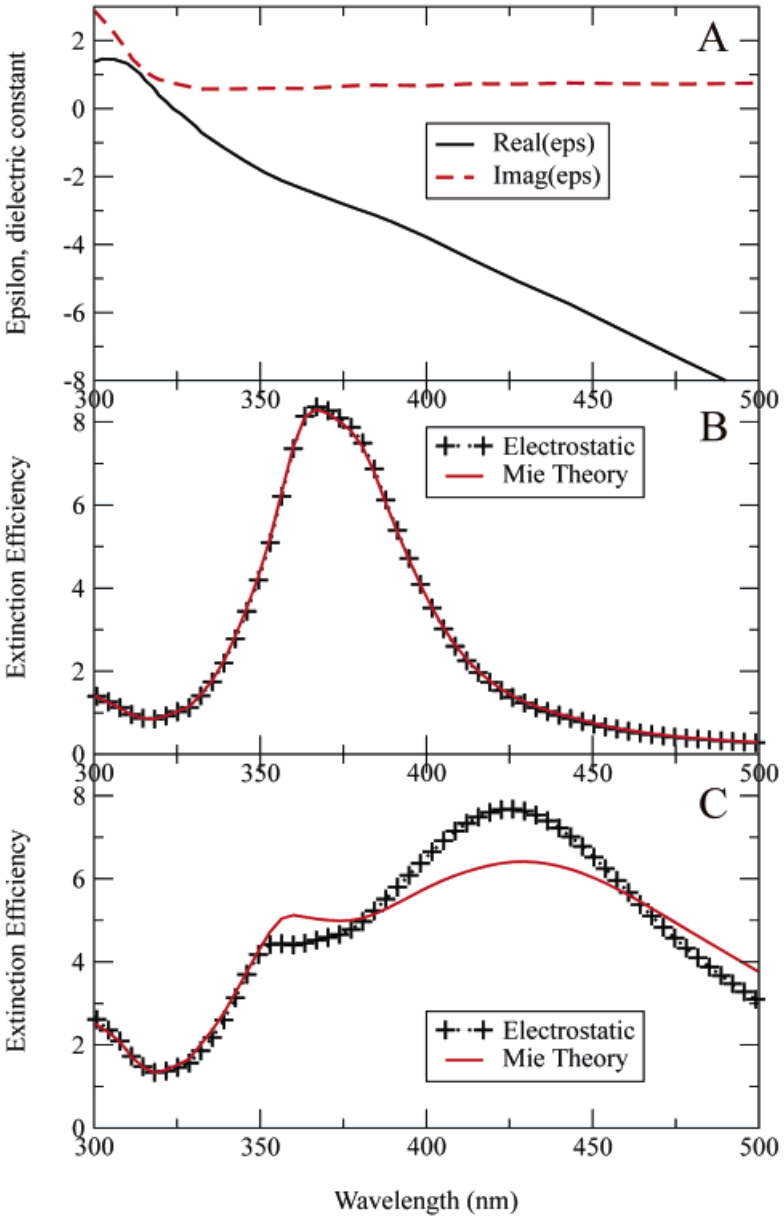

Figure 1.5: Real and imaginary part of silver dielectric constant as a function of wavelengths (A), Extinction efficiency for a 30 nm silver sphere (B), for 60 nm silver sphere (C) [18].

It is well known that a thin film of dielectric sandwiched between conducting layers modulates light intensity due to interference effects. Lian C. T. Shoute et al. [23] have shown the change in intensity and frequency of extinction spectrum of multilayer substrate of silver nanostructures sandwiching dielectric layer in between. In chapter 4, the synthesis of triple layer nanostructures is discussed. The core is made of highly reflecting silica surface while the outer shell is the gold surface and the two layers are separated by a dielectric silica layer. The nanostructure property can be changed by changing the dielectric and the shell thickness. Light incident on the surface of the nanostructure undergoes multiple reflections due to non planar corrugated outer surface. The places where they interfere constructively are the places of high intensity field. Any molecule present at such positions will feel an intense field. Thus these nanostructures are a potential substrate for SERS giving high enhancement factor. Chapter 4 discusses the synthesis and characterisation of such nanoparticles.

In the second part of this chapter, we discuss the effect of capping agent on silver nanoparticles synthesis, stability and SERS. Silver nanoparticles have very high enhancement factor and are popularly used as SERS substrates. But not all silver nanoparticles are equally good for SERS. Depending on the nature of capping agent, the particles stability and efficiency change. Silver nanoparticles capped with three different capping agents were prepared. The capping agents were chosen such that they are different in size and chemical nature. The three different capping agents used are sodium

citrate, polyvinyl pyrrolidone and sodium borohydride and SERS with R6G and Crystal violet were recorded.

1.5 SERS in Bio molecule Detection

Since past few decades, SERS has emerged out as a powerful technique for biomolecule detection and various groups round the world are working in this field. Detection of biomolecules using SERS was done as early as 1980 by Cotton and co workers [24]. Fang et al [25] in 2008 also developed a technique of DNA detection with silicon nanostructure coated with gold and silver, and detection using peptide nucleic acid (PNA) that form a PNA-DNA-Zr. In this case, Zr was linked to rhodamine B and then its SERS was recorded. In the absence of target DNA, the assembly is not formed and hence no SERS is obtained. Another group from Northwestern University has shown that nanoparticles functionalized with oligonucleotides and Raman labels coupled with SERS can be used for multiplex detection of targets oligonucleotides [26].

Several publications with different techniques for DNA detection by SERS method have come up [27-29]. The basic principle behind biodetection is as follows: capture probe biomolecule in the form of DNA or protein / enzyme is immobilised on a substrate. The capture probe being specific to the target goes and binds to the target. The non-bound biomolecules are removed during the wash cycle so only the bound target remains in the solution. A third detector probe containing a Raman active dye and the metal nanoparticles are then added and SERS signal is obtained. The SERS signal is

conclusive of the fact that the target is present while no SERS signal implies that target was not present in the solution. Metal nanoparticles of silver and gold are generally preferred because of their high enhancement factors. Raman active dyes are selected such that their absorption band is in resonance with the surface plasmon resonance of nanoparticles. Further, the application of SERS signal to get maximum sensitivity requires intelligent choice of metal nanoparticles, the Raman active dye and the excitation source.

A major advantage of doing nanoparticles based SERS detection is that we don't have to use radioactive labels as before. But there are some limitations as well. Though numerous SERS studies of DNA have been done, sensitivity and specificity still remain a challenge. In our work, we have tried to deal with the problem of sensitivity by capturing the target oligonucleotide with Fe_3O_4 nanoparticles coated with silica which can be linked to the capture probe oligonucleotide. The size of core shell nanoparticles used is around 200nm while the each magnetic nanoparticles that make the core are 8 nm in size and are superparamagnetic in nature i.e. their retentivity is zero. Once separated, they get well dispersed in the solution after the removal of magnetic field. Using magnetic nanoparticles also make the washing cycle easier without much of a loss in oligonucleotides. Further, silica coating facilitates easy functionalization in order to be linked to the capture probe. This process is a three way detection in which the detector probe and the capture is complementary to a part of target probe oligonucleotide. The detector probe is tagged with a cyanine dye (Cy 5) at the 5′ terminal and an additional

NH_2 at the 3′ terminal while the capture probe's 5′ end is modified with amine group so that it can get attached to the magnetic core silica shell nanoparticle through a linker molecule. Gold nanoparticles prepared by Lee Meisel method is used here. This technique is expected to be highly sensitive and more powerful than the other techniques reported so far.

In coming years, SERS will definitely turn out to be a technique that will be popularly preferred for ultra trace analysis of biomolecules, disease detection etc.

1.6 References

1. Brillouin, L. *Ann. Phys.* (Paris), **1922**, *17*, 88.
2. Raman, C. V.; Krishnan, K. S. *Nature,* **1928**, *121*, 501.
3. Fleischmann, M.; Hendra, P. J.; McQuillan, A. J. *Chem. Phys. Lett.,* **1974**, *26*, 163.
4. Jeanmarie, D. L.; Van Duyne, R. P. *J. Electroanal. Chem.*, **1977**, *84*, 1.
5. Vibrational spectroscopy in life science, Siebert, F.; Hildebrandt, P.
6. The Raman Effect, Long, D. A., John Wiley $ Sons Ltd .
7. Albrecht A.C. *J. Chem. Phys.*,**1961**, *34*, 5, 1476.
8. Warshel, A.; Dauber, P. *J. Chem. Phys.*, **1977**, *66*, 5477.
9. Albrecht, M. G.; Creighton, J. A. *J. Am. Chem. Soc.*, **1977**, *99*, 5215.
10. Campion, A.; Kambhampati, P. *Chem. Soc. Rev.*, **1998**, *27*, 241.
11. Moskovits, M. *Rev. Mod. Phys.*, **1985**, *57*, 783.
12. Otto, A.; Mrozek, I.; Grabhorn, H.; Akemann, W. *J. Phys.: Condens. Matter* **1992**,

4, 1143.

13. Wu, D. Y.; Li, J. F.; Ren, B.; Tian, Z. Q. *Chem. Soc. Rev.,* **2008**, *37*, 1025.
14. Aroca, R. et al., Surface Enhanced Vibrational Spectroscopy (Wiley, West Sussex, **2006**).
15. Rivas, L.; Sanchez-Cortes, S.; Garcı´a-Ramos, J. V.; Morcillo, G. *Langmuir,* **2000,** *16,* 9722.
16. Mansfeld, F.; Smith, T.; Parry, E. P. *Corrosion,* **1971**, *27*, 289.
17. Schweinsberg, D. P.; Bottle, S. E.; Otieno-Alego, V. *J. Appl. Electrochem.,* **1997**, *27*, 161.
18. Kelly, K. L.; Coronado, E.; Zhao, L. L.; Schatz, G. C. *J. Phys. Chem. B,* **2003**, *107,* 668.
19. Khlebtsov, N. G.; Dykman, L. A. *J. Quant. Spectrosc. Radiat. Transfer*, **2010**, *111*, 1.
20. Hao, E.; Schatz, G. C.; Hupp, J. T. *J. of Flourescence*, **2004**, *14*, 4, 331.
21. Murphy, C. J. et al, *J. Phys. Chem. B* **2005,** *109,* 13857.
22. Pillai, Z. S.; Kamat, P. V. *J. Phys. Chem. B,* **2004,** *108*, 945.
23. Shoute, L. C. T. *ChemPhysChem,* **2010**, *11*, 2539.
24. Cotton, T. M.; Schultz, S. G.; Van Duyne, R. P. *J. Am. Chem. Soc*., **1980**, *102,* 7960.
25. Fang, C. et al *Biosensors and bioelectronics***, 2008,** *24***,** 2, 216.
26. Cao, Y. C.; Jin, R.; Mirkin, C. A. *Science*, **2002**, *297,* 1536.
27. Muller, U. R. et al**,** *Biosensors and Bioelectronics***, 2004,** *19*, 8, 875.

28. Hering, K. *Anal Bioanal Chem* , **2008**, *390*, 113.

29. Sun, L.; Yu, C.; Irudayaraj, J. *Anal. Chem.*, **2007**, *79*, 3981.

Chapter 2

Benzotriazoles: A potential system for SERS

2.1 Introduction

Benzotriazoles are an important class of compounds containing a condensed ring system of a benzene and a triazole ring. So far they have been well studied as corrosion inhibitor of copper. The inhibition action happens by forming a protective film of copper triazole polymeric complex at high pH and potential values, and by their adsorption on copper surface at low pH and potential values [1-3]. Benzotriazoles are also used as anti-tarnish agent on silver and are believed to stick by complexing with more than one silver ion to form polymeric species coated on surface [1, 4-6]. This compound, like many other organic compounds, has a hetero atom which can donate electrons and hence act as a base. In addition, it can also undergo electrophilic substitution at the N atom and so different derivatives of benzotriazoles can be prepared by substituting H by other groups. The initial two derivatives synthesized by us have been shown below.

Benzotriazoles have a strong signature in Surface Enhanced Raman Scattering (SERS). The two compounds, the acetate and the acid derivative have been shown to give SERS. The important point to be noted here is that 1H-1,2,3-benzotriazol 1-yl acetic acid is protonated ($-NH^{+}-$) at pH < 1 [7], i.e. it has an overall positive charge, and is deprotonated ($-COO^{-}$) at pH > 5.5 and has an overall negative charge. So depending on

the pH of solution, the compound may be positively charged, neutral or negatively charged. Its interaction with nanoparticle, which is negatively charged, changes as we change the pH and is reflected in the SERS signal. In this chapter we have shown the synthesis of two benzotriazole derivatives from benzotriazole, their Raman spectra and the pH dependent SERS of the acid derivative.

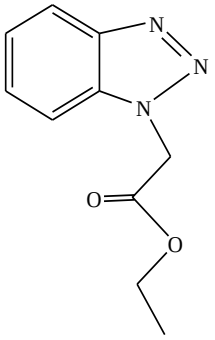

A) Ethyl 1-H 1,2,3-benzotriazol 1-yl acetate (EBTA)

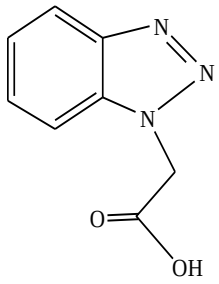

B) 1H- 1,2,3-benzotriazol 1-yl acetic acetic acid (BTAA)

2.2 Experimental Details

Chemicals: Benzotriazole, NaOH and pH 4 buffer were purchased from Merck, DMF was purchased from Qualigens, Ethyl chloroacetate was purchased from Spectrochem, methanol, HCl, LiOH, pH 7 and pH 9 buffer were bought from s.d.fine-chem Ltd. All the chemicals were used as received. Distill water was used for all the preparations.

Synthesis of EBTA: Ethyl 1H 1,2,3- Benzotriazol 1-yl acetate (EBTA) was synthesized by the method given by Alan R. Katritzky and co [8]. Briefly, 4.2mmol of benzotriazole

and 4.2mmol of NaOH was added to a round bottom flask fitted with a calcium chloride guard tube. Further, 4.5ml of DMF and 4.2mmol of ethylchloroacetate was added to the RB and magnetically stirred till the completion of the reaction, which was monitored by TLC. Then the reaction mixture was poured into water and the oily products were extracted with ethyl acetate. Column was done to separate the two fractions. The reaction is shown below.

Reaction 1:

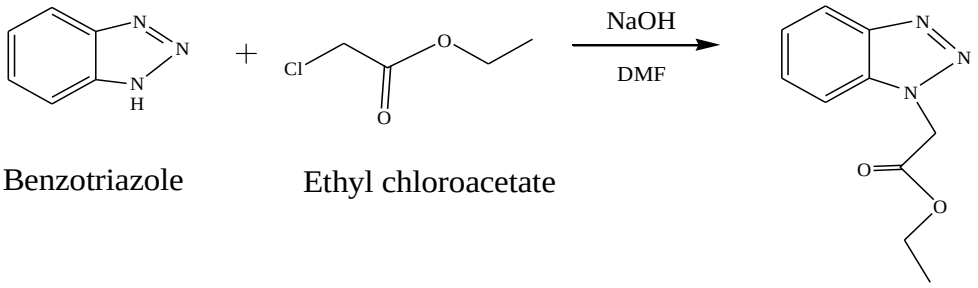

Benzotriazole Ethyl chloroacetate

1H 1,2,3-benzotriazol 1-yl acetic acid

Synthesis of BTAA: 1H-1,2,3-benzotriazol 1-yl acetic acid was synthesized by basic hydrolysis of ethyl 1H-1,2,3-benzotriazol 1-yl acetate (ester). Briefly, 3.2ml of methanol was added into the RB containing 200mg of the above synthesized ester and magnetically stirred for 5 min. Then 61.4mg of LiOH dissolved in 1ml water was added to the RB and stirred continuously for 1 hr. After the completion of reaction, methanol and water was evaporated from RB, in rotavapor. Then 1N HCl was poured into the RB and finally the acid was extracted with ethyl acetate. The reaction has been shown below.

Reaction 2:

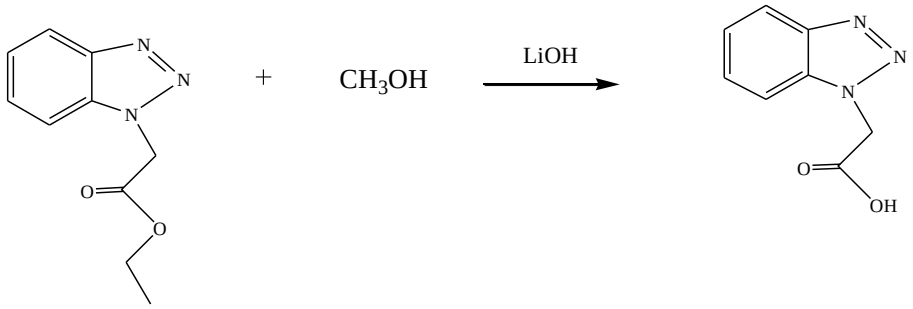

Ethyl 1H 1,2,3-benzotriazol 1-yl acetate

1H 1,2,3-benzotriazol 1-yl acetic acid

Sample preparation: Silver nanoparticles were prepared by Lee Meisel method [9] and centrifuged (to concentrate the nanoparticles) before use. 1mM concentration of the benzotriazole derivatives was made in water. For SERS, the organic compound and the silver nanoparticle was mixed in an appendorf in the ratio 1:10 and from this 1µL was withdrawn and dropped on a clean glass slide and allowed to dry before taking spectra.

For SERS at different pH, the organic compound was dissolved in the different buffer solutions obtained commercially. This was then mixed with centrifuged and concentrated silver nanoparticles in the same ratio as discussed before. Spectra were taken with red laser 633nm, unless otherwise specified. For recording Raman spectra, powder sample of both the organic compounds were used.

2.3 Results and Discussions

Ethyl 1H 1,2,3-benzotriazol 1-yl acetate(ester) and 1H 1,2,3-benzotriazol 1-yl acetic acid (acid) were synthesized. The synthesis was confirmed by NMR and TOF-MS. For Ethyl 1H 1,2,3-benzotriazol 1-yl acetate, ^{1}H NMR (400MHz, $CDCl_3$) δ: 1.26 (t, *J*= 7.14, 3H, CH_3), 4.25 (q, *J*=7.13, 2H, CH_2), 5.40 (s, 1H, CH_2) and medium intensity peaks corresponding for aromatic protons at δ: 7.39 (t, *J*=7.49, 1H, Ar-H), 7.50 (m, *J*=9.97, 2H, Ar-H), 8.08(d, *J*=8.32, 1H, Ar-H) and the molecular ion peak in TOF-MS occurred at 205. For 1H 1,2,3-benzotriazol 1-yl acetic acid, ^{1}H NMR (400MHz, DMSO-d_6) δ: 5.25 (s, 2H, CH_2), 7.23 (m, *J*=6.64, 1H, Ar-H), 7.36 (m, *J*=7.63, 2H, Ar-H), 7.88(d, *J*=8.35, 1H, Ar-H) corresponding to the aromatic protons of benzene ring. The reference compound was tetramethylsilane for NMR measurements. TOF-MS gave the molecular ion peak at 177 confirming the presence of acid.

2.3.1 Raman of EBTA and BTAA

Raman spectra of the powder (solid) sample of EBTA and BTAA were taken using a laser light of incident wavelength 633nm. The accumulation time for each spectra were 60s. Figure 2.1 and Figure 2.2 shows the Raman spectra of solid ethyl 1H-benzotriazol 1-yl acetate and 1H benzotriazole 1-yl acetic acid respectively, in the frequency range 800-1800cm^{-1}.These spectra were smoothed with 10% cut off FFT filter. Baseline correction was done using 10 point Positive Peak Algorithm in origin. For the recorded spectra, important peaks have been assigned and shown in the Table 1. The data is consistent with

the previous reported works on other benzotriazole derivatives[8, 10-13]. We can clearly see that apart from the signature peaks of benzotriazole which are due to the

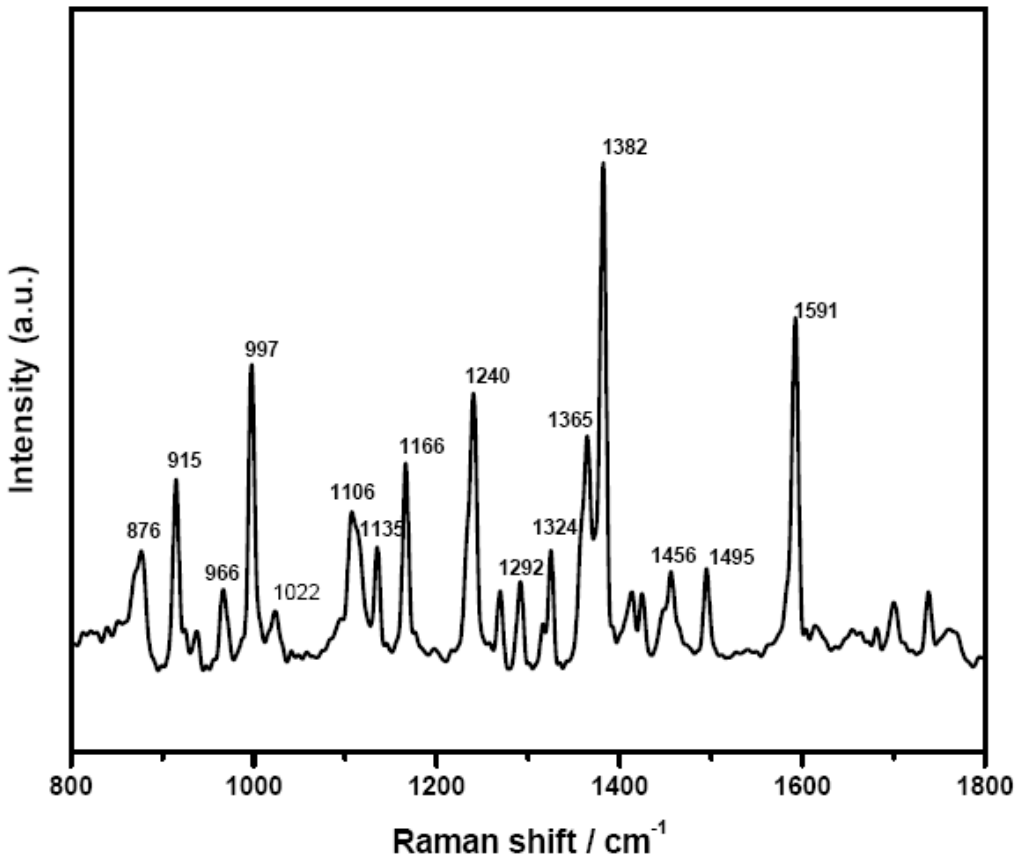

Figure 2.1: Raman spectra of ethyl 1H 1,2,3-benzotriazol 1-yl acetate with 60s accumulation time.

benzene ring stretching (1499, 1596 cm^{-1}), bending (1002 cm^{-1}), breathing modes and triazole modes (1166, 1236 cm^{-1}); there are peaks corresponding to C=O stretch (1701 cm^{-1}), C-O stretch (1324 cm^{-1}), CH_2 wag and twist (1139 cm^{-1}) of the benzotriazole acetate (EBTA) and the acid (BTAA). For the acid, BTAA there is very strong peak at 1172 cm^{-1} for the C-OH stretch. Some peaks in the acid were observed to have shifted by

5 - 6 cm^{-1} with respect to the ester peaks. This may be due to the change in polarizability of the molecule as the acid is more polar than the ester. The 1405 cm^{-1} peak corresponds to symmetric COO^- stretching of the acid. One can also see that this peak is missing in the ester.

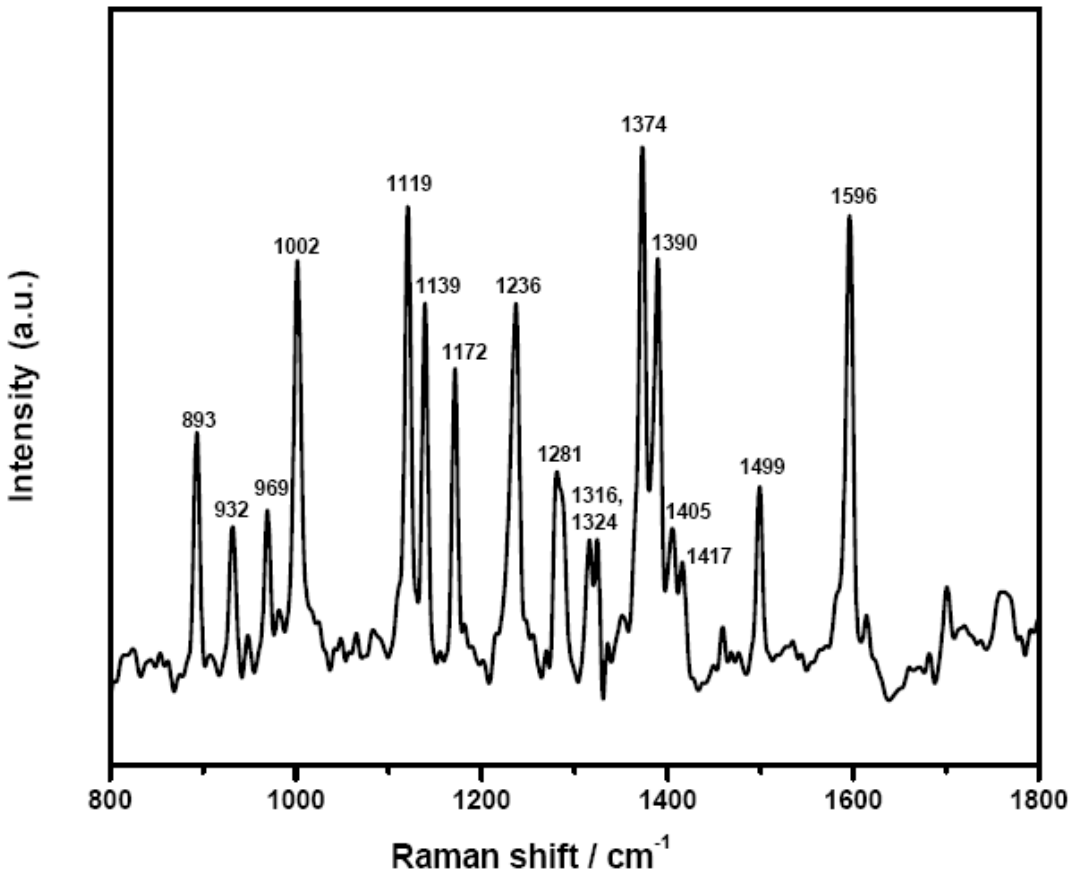

Figure 2.2: Raman spectra of 1H 1,2,3-benzotriazol 1-yl acetic acid with 60s accumulation time.

Table 1: Peak assignment for the Raman of solid sample EBTA and BTAA.

Ethyl 1H 1,2,3-benzotriazol 1-yl acetate (EBTA) (cm^{-1})	1H 1,2,3-benzotriazol 1-yl acetic acid (BTAA) (cm^{-1})	Peak Assignment
876	-	
-	893	
915	-	
938	932	γ-CH,C-OH bend
966	969	
997	1002	δ-Bz skeletal
1022	-	Ring str
1106	1119	Tz mode
1135	1139	CH_2 wag & twist
1166	-	v_{as} N-N-N
-	1172	C-OH str
1240	1236	Tz ring breathing
1269	1281	δ-CH
1292	-	δ-CH
1313	1316	
1324	1324	v C-O
1365	-	v-Bz ring
1382	1374	v-Bz ring
-	1390	v-Tz ring
-	1405	v_s-COO^-
1413	1417	
1425	-	δ Me
1456	-	δ Me, v-Ph
1495	1499	v-Bz ring str
1591	1596	v-Bz ring str
1699	1701	C=O str

Bz: benzene, Tz: triazole, str: stretching, v_s:symmetric vibration, v_{as}: asymmetric vibration, γ:out of plane bending, δ: in plane bending.

2.3.2 Variation in SERS of BTAA with pH

BTAA can behave differently in different pH environment. 1H 1,2,3-benzotriazol 1-yl acetic acid molecule is both an electron donor (though N) and proton donor from the acetic acid end and so behaves differently at different pH. The 3-N in the triazole ring has a pKa <1, while the acetic acid has pKa ~ 5. According to Henderson Hasselbalch equation we have,

$$pH = pK_a + log\frac{A^-}{HA}$$

...2.1

which shows the behavior of acid with different pH. For pH < pKa, the molecule is protonated while for pH > pKa, the molecule is deprotonated and for pH = pKa, the protonated and the deprotonated form are in equilibrium with each other. So the molecule can either be negatively charged, neutral or positively charged depending on its pH. Further, its interaction with the nanoparticle, which is negatively charged, will change as the net charge on the molecule changes. This change is reflected in SERS spectra of BTAA molecule at different pH. Three different pH buffer solutions, pH 4, pH 7 and pH 9 were used for this study. 1mM concentration of compound was prepared in the buffer solutions and used for SERS. To confirm that the signal is not of buffer, blank test with buffer solutions were performed. Silver nanoparticles prepared by citrate reduction of silver nitrate were used for all the studies. The pH of the silver nanoparticles was also

brought to the pH under consideration by addition of HCl or NaOH. To increase the concentration of silver nanoparticles per ml, 1 ml of silver nanoparticles were centrifuged and the supernatant was thrown so that the final volume is reduced to 100µL. These nanoparticles were then sonicated to make a uniform solution. For blank test, SERS of buffer solution was taken and the experimental conditions were kept same as that while taking the SERS spectra of the molecule. Figure 2.3 shows the SERS spectra of the buffer and that of the BTAA molecule in pH 4 buffer at a concentration of 1mM. It can be seen that the peaks at 1125, 1384, 1460, 1601 cm^{-1} of the molecule is overlapping with the buffer peak at 1128, 1381, 1463, 1605 cm^{-1} repectively. The nanoparticle to buffer ratio has been kept constant in both the cases. So these peaks can be ignored to some extent as their intensity is low as compared to the peaks of the molecule, though they both contain same volume of buffer. It can be said that buffer is also binding to the nanoparticle quite effectively. But in the presence of molecule there is competition between the molecule and the buffer towards binding to the nanoparticle.

It is evident from the Fig 2.3 that the molecule is binding more efficiently to the nanoparticle and its Raman signal is enhanced. Comparison of the solid Raman spectra and SERS shows some differences in the peak positions and the intensity. Characteristics triazole modes in the solid at 1119, 1236, 1390 cm^{-1} are enhanced but shifted to 1102, 1232, 1384 cm^{-1} respectively. So triazole moiety of the molecule BTAA must be closer to the nanoparticle and the vibrational modes are perpendicular to the surface of the silver nanoparticle. The decrease in relative intensities of some of the vibrational modes of

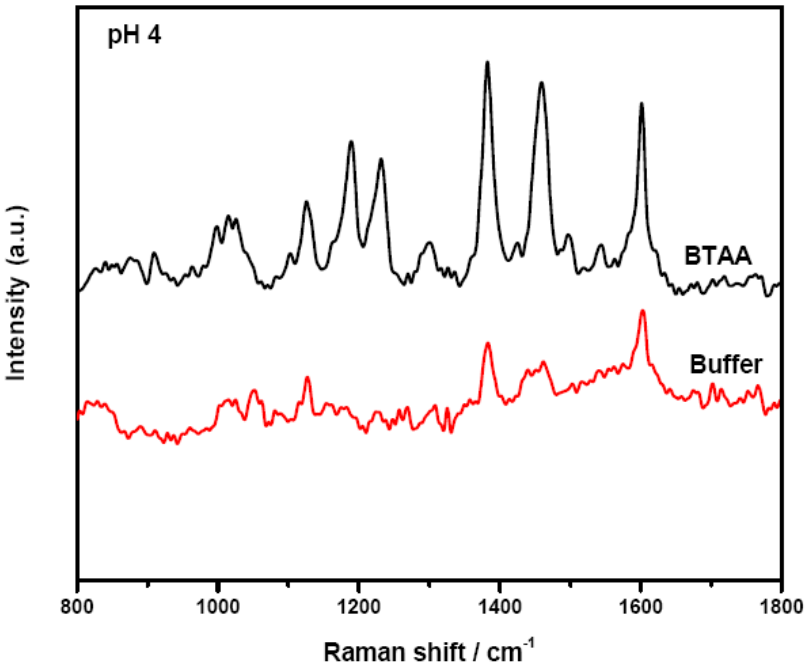

Figure 2.3: SERS spectra of 1H 1,2,3-Benzotriazol 1-yl (BTAA) in pH 4 buffer solution at 1mM conc and of pH 4 buffer (blank).

benzene (1498, 994 cm^{-1}) and the disappearance of 1374 cm^{-1} benzene ring stretching frequency augments the above observation. The strong peak at 1190 cm^{-1} suggests that N is protonated. So the molecule at acidic pH has the tendency to get protonated at N of the triazole group and this group is nearer to the nanoparticle. All the bands observed in the SERS spectrum of BTAA molecule at different pH have been assigned and given in Table 2.

Figure 2.4 shows the SERS spectra of the pH 7 buffer and the molecule BTAA at this pH. Here there is least or almost no overlap between the two spectra and many modes can be seen in the figure. The molecule at this pH is expected to be neutral. All the triazole modes at 1122, 1238, 1388 cm^{-1}, the benzene modes at 994, 1362, 1605 cm^{-1} and the v-

CO modes at 1197, 1327 cm^{-1} are seen but they have much lesser intensity as compared to the Raman or SERS intensity of BTAA at other pH conditions. This suggests that the molecule does not have any preferable binding site and its orientation on the nanoparticle is also random. The absence of buffer peaks in the BTAA spectra shows the molecule binds better to the nanoparticles compared to the buffer molecules.

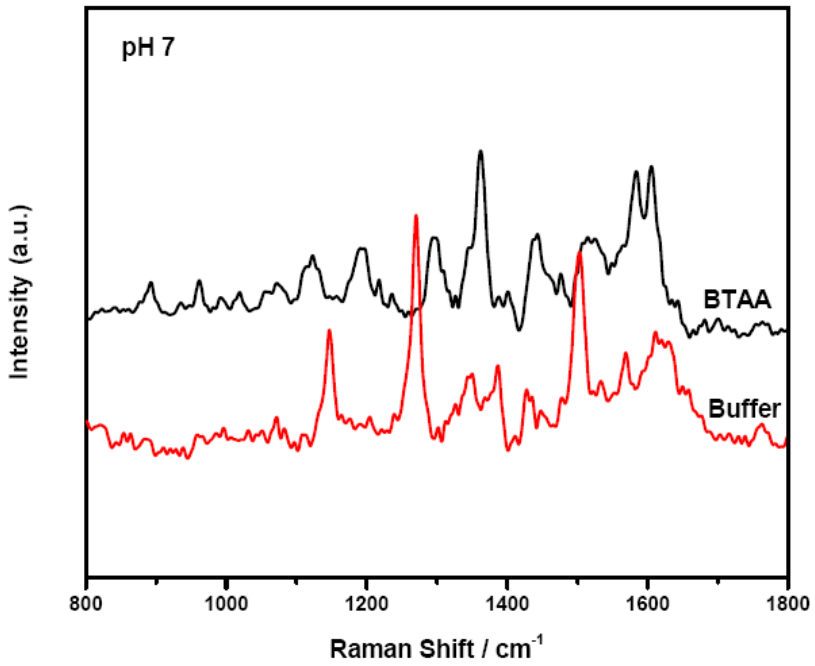

Figure 2.4: SERS spectra of 1H 1,2,3-Benzotriazol 1-yl (BTAA) in pH 7 buffer solution and of pH 7 buffer (blank).

SERS of BTAA at pH 9 and the buffer is shown in figure 2.5. Here too we can see lot of overlap between the buffer bands and the molecule bands but we can avoid them for reasons mentioned above. Modes corresponding to benzene and triazole ring are seen

here but with reduced intensity as compared to its Raman spectra and SERS at pH 4 and pH 7. On the other hand one can see very intense peak at 1270 cm^{-1} corresponding to C-O stretching. This band was absent at pH 4 and pH 7, and had very weak intensity in Raman. In addition, the CH_2 wag and twist also had its signature in the spectrum at 1148 cm^{-1}, this peak also had very low intensity in the Raman signal of the molecule. Hence, we can say that at pH 9 the molecular interaction to the nanoparticle is happening through the carboxyl portion of the molecule. Thus the benzotriazole group is standing away from the nanoparticle surface.

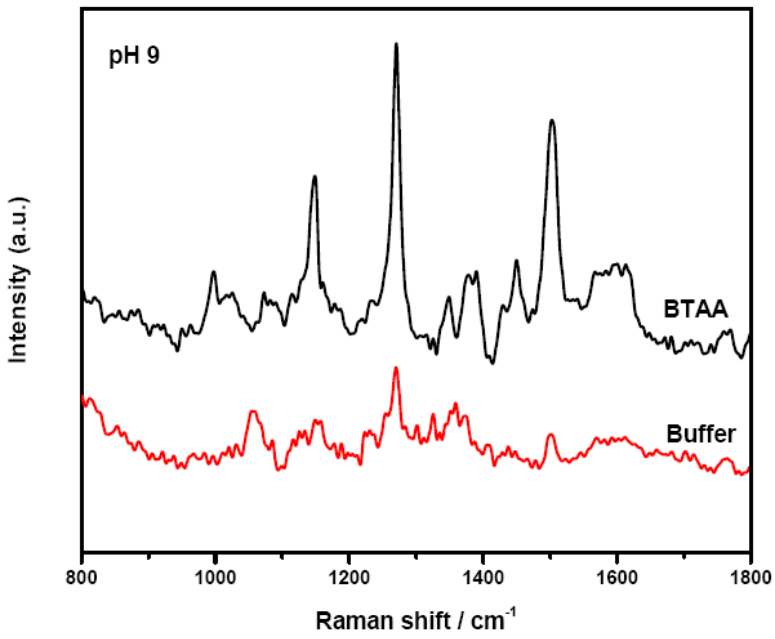

Figure 2.5: SERS spectra of 1H 1,2,3-Benzotriazol 1-yl (BTAA) in pH 9 buffer solution and of pH 9 buffer (blank).

The BTAA molecule behaves differently in different pH environment in the sense that some bands appear in one pH while it disappears in other pH. The peak intensity also changes drastically at different pH and is dependent on the orientation of the molecule on the nanoparticle. The groups of the molecule which is nearer and whose orientations

Table 2: SERS peak (in cm^{-1}) and peak assignments of BTAA at different pH.

pH 4	pH 7	pH 9	Peak assignment
994 w	994 w	999 w	bz ring str
1102 w	-	-	tz mode
1125 s	1122 m	1127 hump	tz mode
-	-	1148 m	CH_2 wag & twist
1190 s	1196 m	-	C-OH str
1232 s	1238 vw	-	tz mode
-	-	1270 vs	CO str
-	1297 s	-	δ-CH
-	1327 vw	-	ν-CO
-	-	1348 m	
-	1362 s	1376 m	bz ring str
1384 vs	1388 vw	1390 m	tz mode
-	1401 w	-	sym COO str
1426 w	1440 s	1448 m	ν-skeletal
1460 s	1462 hump	-	bz ring str
1498 w	-	1505 s	bz ring str
-	1583 s	-	ν-skeletal
1601 vs	1605 s	-	bz ring str

Bz: benzene, Tz: triazole, str: stretching, v_s:symmetric vibration, v_{as}: asymmetric vibration, γ:out of plane bending, δ: in plane bending.

are perpendicular to the nanoparticle are enhanced more compared to the other modes. This was clearly seen in the pH dependent SERS studies done above. The CH_2 wag and twist mode at 1148 cm^{-1} and C-O stretching mode at 1270 cm^{-1} present in pH 9 are absent in pH 4. The triazole modes at 1232 and 1384 cm^{-1} present in pH 4 are either reduced in intensity or absent in the pH 9. Also, the benzene modes that are present in pH 4 are absent in pH 9 and vice versa, like benzene ring stretching frequency at 1601 cm^{-1} has a very strong peak in pH 4 whereas it is absent in pH 9, the 1505 cm^{-1} benzene stretching frequency present in pH 9 has a very low intensity in pH 4 . So, this molecule can act as a pH sensor molecule exhibiting Raman scattering characteristics to pH. Put in an unknown environment it can tell us the pH of the system. It can also be conjectured that going from one pH environment to other would change the spectra and again coming back to the same environment would give the same spectra of that pH. This cycle should be repeatable and it is possible to predict the change in pH environment as we are moving from one point to another in any biological system depending on the change in SERS spectra.

2.4 Conclusions

We have shown the preparation and characterization of two organic molecule which are derivatives of benzotriazole, namely ethyl 1H 1,2,3-benzotriazol 1-yl acetate and 1H 1,2,3-benzotriazol 1-yl acetic acid. Here, for the first time we have shown the Raman spectra of these two molecules. Both the synthesized molecules have very good signature

peaks of the benzene ring, triazole moiety and the acetic acid/ acetate group. The SERS spectra of the 1H 1,2,3-benzotriazol 1-yl acetic acid at different pH is shown. It is clear from the SERS spectra that the molecule has different charge at different pH. Depending

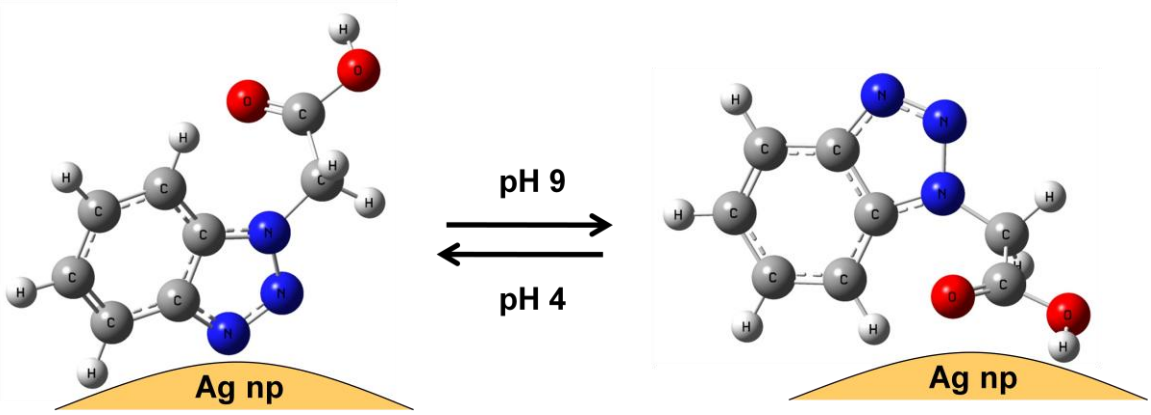

Figure 2.6: Conformation of BTAA at the silver surface at different pH.

on this charge, the orientation of the molecule on the nanoparticles surface also changes as shown in figure 2.6. This change in orientation is reflected in the SERS spectra. At acidic pH the molecular interaction with the silver nanoparticle takes place via the N of the triazole group in vertical or tilted orientation. So the triazole modes are more enhanced whilst rest other modes are suppressed. At basic pH, the interaction takes place through carboxyl group, so carboxyl modes and CH_2 modes can be seen whereas these modes are not present at other pH. At neutral pH, it is difficult to say the interaction site in the molecule as almost all the modes with weak or moderate intensity are seen. This molecule can be used as pH sensor molecule for basic, acidic as well as neutral pH. By

looking at the spectra, the pH environment in the near vicinity of the molecule can be predicted. So benzotriazole acetic acid can be very useful in studying a biological system.

Future Scope

As discussed before, 1H 1,2,3-benzotriazol 1-yl acetic acid SERS depends on the pH of the environment in which it is present. So, oligonucleotides can be tagged with the benzotriazol 1-yl acetic acid derivative so that one end has benzotrizole group while the other end has acetic acid. Both the end groups can be separated from the oligonucletide sequence by spacer methylene groups. The oligonucleotide sequence is such that the two end sequences are complementary to each other. Now it is speculated that in absence of any complementary sequence, the capture probe forms a stem loop kind of configuration keeping –COOH and BTA groups together. In acidic pH, this configuration will orient itself on the nanoparticles such that binding happen through the triazole moiety and peaks corresponding to triazole groups are more enhanced. After hybridisation happens, the loop opens up. Now the –COOH and Tz group are far apart but still Tz peaks would be seen. At basic pH, the binding happens through COOH group. So before hybridisation only benzene, methylene and carboxyl peaks would be predominantly seen whilst after hybridization when the loop opens, the double stranded oligonucletide being a long chain may curl up in a manner so as to bring the Tz moiety nearer to the nanoparticles, so in addition to peaks seen earlier one would also see Tz modes indicating the presence of

target in the sample. This technique can be efficiently used for DNA detection process by utilizing the switching behaviour of benzotriazole molecule and observing the change occurring in the SERS spectrum.

2.5 References

1. Ling, Y.; Guan, Y.; Han, K. N. *Corrosion*, **1995**, *51*, 367.
2. Wu, Y. C.; Zhang, P.; Pickering, H. W.; Allara, D. L. *J. Electrochem. Soc.*, **1993**, *14*, 2791.
3. Xue, G.; Ding, J.; Lu, P.; Dong, J. *J. Phys. Chem*.,**1991**, *95*, 7380.
4. Wilson, H.; Smith, W. E. *J. Raman Spectroscopy*, **1994**, *25*,899
5. Rubin, J. C. *Chem. Phys. Lett*., **1990,** *167*, 209.
6. Graham, D. et al *Chem. Comm*., **1998**, 1187.
7. Schweinsberg, D. P.; Bottle, S. E.; Otieno-Alego, V.; Notoya, T. *J. of Appl. Electrochem.*, **1997**, *27*, 161.
8. Katritzky, A. R.; Kuzmierkiewicz, W. ; Greenhill, J. V. An improved method for the N-alkylation of benzotriazole and 1,2,4 triazole, **1991**, 369.
9. Lee, P. C.; Meisel, D. *J. Phys. Chem.* **1982**, *86*, 3391.
10. Zhang, P.; Liang, E.; Li, X. *Chinese Phy. Lett.* **1988**, *5*, 329.
11. Bigotto, A.; Pandey, A. N.; Zerbo, C. *Spectroscopy Lett.*, **1996**, *29*,511.
12. Rubin, J.; Gutz, G. R.; Sala, O.; Orville-Thomas, W. J. *J. Mol. Struct.*, **1983**, *100*, 571.

13. Chan, H. Y. H.; Weaver, M. J. *Langmuir,* **1999**, *15*, 3348.

14. Rava, R. P.; Spiro, T. G. *J. Am. Chem. Soc*, **1984**, *106*, 14, 4062.

Chapter 3

Nanostructures

3.1 Introduction

Nanoparticles have become the core of today's research. Metal or metal-organic/inorganic composite nanoparticles are class of materials widely used in the fields of colloid and materials science due to their unique and tailored properties for various applications as catalysts, sensors, surface enhanced Raman or resonance Raman scattering substrates etc [1-4]. In the last few decades, there have been many efforts in developing various synthesis procedures for producing nanoparticles. Recently, the attention has shifted to core shell nanoparticles due to ease of manipulation of morphologies, compositions and surface functionalisations, which facilitate its use for different purposes. The shell can alter the charge, surface reactivity, functionality and stability of the core. Moreover, desired functionalities like optical, magnetic or catalytic can be imparted to nanoparticles by the suitable choice of core and the shell.

Nanoparticles have very high surface to volume ratio and due to this, its properties change as we go from bulk to nano. These properties become very interesting at nanoscale and can be harnessed for various applications. Among the various nanopaticles, metal nanoparticles are gaining popularity due to their important optical and electronic properties. These nanoparticles support surface plasmons (collective excitation

of conduction electrons as induced by electromagnetic field) [5]. For metal nanoparticles like gold and silver, the surface plasmon resonance (SPR) occurs in the visible region. This SPR frequency of nanoparticles is different from bulk and can be changed, depending on our requirement, by changing the size [6], shape [7], aggregation [8], structure [9] and dielectric properties of the surrounding medium [10]. Figure 3.1 shows the SPR range for silver and gold nanoparticles having different morphologies,

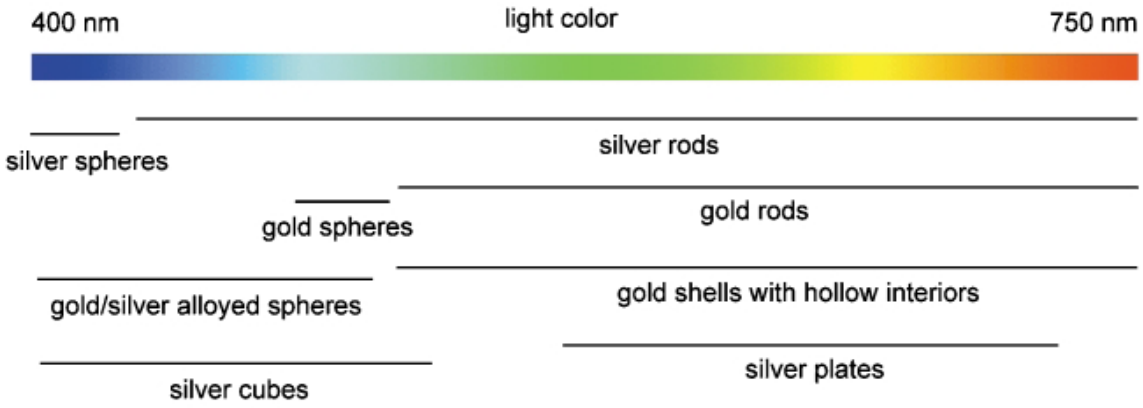

Figure 3.1: SPR band of different nanoparticles [11].

compositions and structures [11]. The tuning of SPR of nanoparticles by changing morphology find extensive application as medium for electron transport and charging [12], as probes for scanning near field optical microscopy [13], as substrates for surface enhanced Raman scattering (SERS) [14] or fluorescence scattering [15], and for chemical and biological sensing [16].

Core shell nanoparticles, especially metal core silica shell nanoparticles have attracted a deal of attention due to the ease of functionalization of the shell. The shell can be easily modified to be linked to a biomolecule or, a marker molecule can be incorporated within the silica shell to make a composite structure. The shell also protects the core by preventing its interaction with the surrounding environment, while retaining its inherent property. Moreover, silica shell itself is quite stable to different acidic or basic environments. Due to these advantages, there have been lots of efforts into developing silica coated metal nanoparticles. Liz-Marzan and Ung gave a three step synthesis procedure to make metal (gold or silver) core silica shell nanoparticles [17,18]. Lu et al [19] demonstrated a modified Stober process [20] to prepare iron oxide core silica shell nanoparticles that show a combination of magnetic and optical properties. Wang et al reported an easy fabrication method for hollow Ag/ SiO_2 double shelled spheres [21].

The growth of silica shell on metal/metal oxide nanoparticles involves base-catalyzed hydrolysis of tetraethyl orthosilicate (TEOS) and subsequent condensation onto the surface of metal nanoparticles. The maximum shell thickness and growth rate are influenced by the amount of TEOS added and the ratio of water to alcohol (ethanol or propanol) used.

In this chapter, I have discussed the synthesis and characterization of core shell nanoparticles with different metallic core and silica shell. The main aim behind this

synthesis is to obtain a nanoparticle system that would give a better SERS enhancement factor than the existing nanoparticles.

3.2 Ag@SiO2@Au nanostrucutres

A thin film of dielectric sandwiched between two reflecting layers can modulate the light intensity by interference effects. The frequency as well as intensity of extinction spectrum varies enormously with the change in the intermediate layer thickness. Thus, one can modulate the absorption frequency by changing the interlayer spacing, the metal of which the reflecting layer is composed and the thickness of reflecting layers. As mentioned before, our aim is to synthesize a nanostructure that would give better SERS enhancement factor. Figure 3.2 shows the schematic for a planar three layer nanostructure that can lead to increased Raman intensity [22].

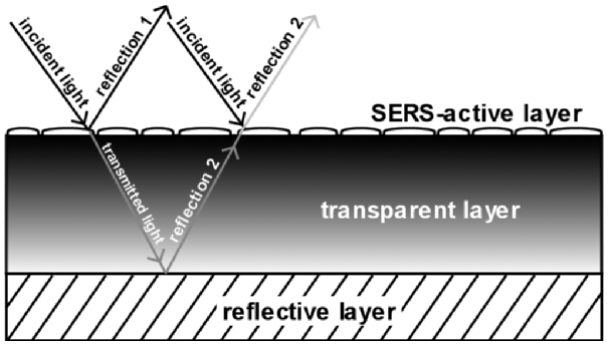

Figure 3.2: Schematic for interference in three layer structure leading to increased Raman intensity [22].

3.2.1 Experimental Details

Chemicals: Silver Nitrate, 3-aminopropyl triethoxysilane (APTES) and tetrakis hydroxymethylphosphonium chloride (THPC) were purchased from Sigma Aldrich; poly N-vinyl pyrrolidone, PVP was purchased from Loba Chemie; absolute ethanol from Commercial Alcohols; sodium hydroxide, tetraethyl ortho silicate (TEOS) and ammonia solution (28-33%) were purchased from Merck, K_2CO_3 from s.d.fine-chem Ltd and hydroxylamine hydrochloride from Qualigens were purchased. For all the preparations, milli Q water was used.

Preparation of Ag@SiO_2@Au nanoparticles

The core Ag@SiO_2 was prepared by the method given by Chaorong Li et al [23]. Briefly, 100 ml of absolute ethanol and 50 ml of milli Q water was vigorously stirred at 75^o C. To this, 10 ml of 0.05 M aqueous solution of silver nitrate was added and stirred for 5 min and heating was continued. Then 20 ml of 2.5 mM PVP was added in aliquots of 1 ml, in 5 min. After the mixture was stirred for 20 min at 80^o C, 5 ml of 0.1 M NaOH was added to the solution. The solution was cooled while stirring was continued for 2 hrs after which silver nanoparticles were obtained.

For silica coating, 50 ml of absolute ethanol, 5 ml of ammonia solution, and 1 ml of TEOS were added to the PVP capped silver nanoparticles. This solution was stirred overnight (12 hrs) at room temperature. The Ag@SiO_2 nanoparticles formed were washed with 1:1 solution of ethanol and water. To get different thickness of silica coating, the amount of TEOS was varied.

Gold coating over $Ag@SiO_2$ nanoparticles were done by using a modified approach given by Christina Graf et al [24]. 50 mg of the above synthesized $Ag@SiO_2$ nanoparticles were suspended in 2 % solution of 3- aminopropyl triethoxysilane in ethanol. This was then washed with ethanol and resuspended in 50 ml fresh ethanol. For the gold coating, first 1-2 nm gold nanoparticles were deposited on the $Ag@SiO_2$ nanoparticles. The gold nanoclusters were prepared by the adopting the method given by Duff. et al [25]. Briefly, 45.5 ml of water was put in 100 ml RB. To this, 1.5 ml of 0.2 M NaOH was added while stirring. 1.2 ml of 80 % aqueous solution of THPC was diluted to make 100 ml. 1 ml of this diluted THPC solution was added to the RB. Then 2 ml of 25 mM dark aged solution of $HAuCl_4$ was added to the above mixture resulting in the formation of orange brown hydrosols of gold. 2 min interval was allowed between the addition of $HAuCl_4$ and THPC.

The APTES modified $Ag@SiO_2$ nanoparticles (50 ml) were added drop wise to the gold nano particle solution in 10 min. The solution was stirred for 12 hrs. Non attached gold nanoparticles were removed by centrifugation at 4000 rpm. Washed nanoparticles were redispersed in 100 ml water, stirred for 1 hr to form a uniform colloidal solution and kept for ageing in fridge at 4^oC for a week.

A 3.48 ml of 25 mM $HAuCl_4$ was diluted with water to 200 ml and to this 49.8 mg of potassium carbonate was added and aged for 1 day. The precursor $Ag@SiO_2$ nanoparticles decorated with gold nanoparticles were added to the aged solution of $HAuCl_4$ / K_2CO_3 and stirred for 10 min. Then, a freshly prepared solution of

hydroxylamine hydrochloride (0.013g in 100 ml water) was added drop wise to the above solution in 45 min. The color of nanoparticles changed from black to brown.

Characterizations: Transmission electron microscopy (TEM) measurements were performed using JEOL 3010 with an operating voltage of 300 keV. UV-Vis measurements were done using Perkin-Elmer Lambda 900 UV / Vis / NIR spectrometer. SERS measurements were performed by a custom-built Raman microscope. In the present experiment red laser with 633nm wavelength was used. The laser power near sample was around 10 mW.

3.2.2 Results and Discussions

Ag@SiO_2@Au nanostructure was prepared and characterized. TEM of the core shell nanoparticles at the different stages of formation has been shown in the figures below. Figure 3.3 shows uniform coating of silica over silver nanoparticles with particle size between 90-100 nm. There are four steps for the synthesis of Ag@SiO2@Au nanostructure as mentioned before and for each step mechanism has been discussed in the following paragraphs. First, PVP capped silver nanoparticles are prepared. These nanoparticles are quite stable over a long period of time, in comparison to those prepared by other methods. Second step is the silica coating over silver nanoparticles and its mechanism goes like this. TEOS in presence of ethanol and ammonia solution is hydrolyzed to form $Si(OH)_4$, which condenses over time and forms silica. Silica film

thickness depends on the amount of TEOS added and pH of the solution [26]. To remove small silica nanoparticles formed in the process, the nanoparticles solution is centrifuged at 4000 rpm so that only core shell nanoparticles settle down whereas silica nanoparticles remain in the supernatant and can be removed. Here it must be made clear that only polymer capped silver nanoparticles can be used to get a uniform silica coating. The coating could not be done on citrate capped nanoparticles as they are not very stable. Though coating did happen on some of the citrate capped nanoparticles, it was not uniform and many silica nanoparticles without core were seen to be formed. Figure 3.3 shows the TEM image of silver core silica shell nanoparticles.

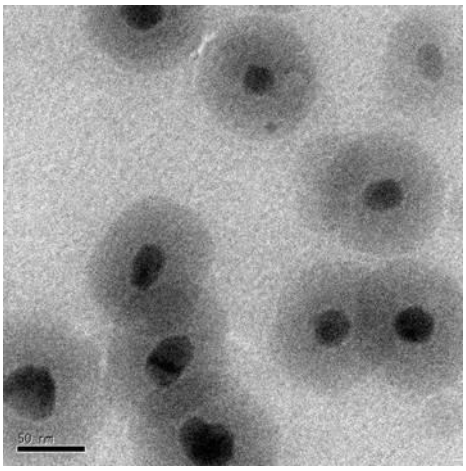

Figure 3.3: TEM image of silver core silica shell nanoparticles.

Third step is the creation of nucleation sites for growth of gold shell. Gold has very little affinity for silica. So, silane coupling agent 3-aminopropyl triethoxysilane (APTES) is used to modify the surface of silica. Hydrolysis of this material produces methanols and

trisilanols while the Si-C bond is still intact. This bond is hydrolytically stable and the aminopropyl group will not be cleaved. The transient silanol groups will condense with other silanols and as a result aminopropyl functions on silica surface are generated. The strong chemical affinity of primary amines for gold causes the chemisorption of gold colloid on silica surface through the amino group. Thus, $Ag@SiO_2$ nanoparticles studded with gold nanoparticles (1-2 nm) are formed. TEM picture of the nanoparticles has been shown in the figure 3.4.

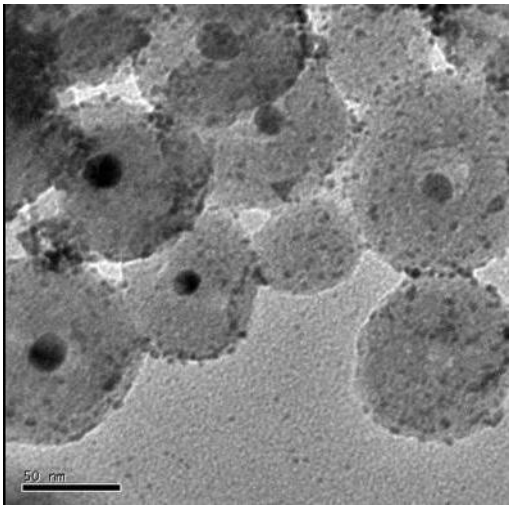

Figure 3.4: TEM image of $Ag@SiO_2$ studded with gold nanoparticles.

Next step is the growth of gold shell on the above nanoparticles. This was brought about by adding the precursor $Ag@SiO_2$ nanoparticles covered with gold cluster to the aged solution of aurochloric acid and potassium carbonate. Since there are gold sites already present on the silica shell, so the newly added gold ions would get reduced at those sites

only. Besides, the new nucleation of gold nuclei should also be prevented. This requires a reducing agent which reduces gold salts only on already existing gold surface. This job is done by using hydroxylamine as a reducing agent. Figure 3.5 shows the TEM image of the $Ag@SiO_2@Au$ nanostructure. Here also, for those core shell nanoparticles where small gold nanoparticles were not attached, growth of gold shell did not take place. So in TEM image one can also see the $Ag@SiO_2$ nanoparticles with no gold shell. The non-coated silica shell can be removed by centrifugation to get pure $Ag@SiO_2@Au$ nanoparticles.

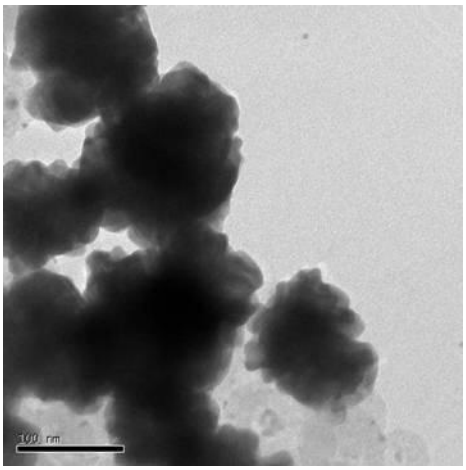

Figure 3.5: TEM image $Ag@SiO_2@Au$ nanostructure.

These nanoparticles were used as substrates for SERS. He-Ne laser (633nm) was used as the excitation beam and the accumulation time was 30 sec. Rhodamine 6G was used as test molecule. SERS spectrum was obtained for 10^{-5} M R6G and is shown in figure 3.6. The peaks at 1360, 1504, 1570 and 1648 cm^{-1} correspond to aromatic C-C str. Peaks at

1126 and 1269 cm^{-1}, which are quite weak in intensity and can be assigned to C-H in plane bend and C-O-C stretching frequencies respectively [27, 28]. Peak at 613 cm^{-1} is due to C-C-C ring in plane bend. SERS of 10^{-6} M R6G were very weak in intensity.

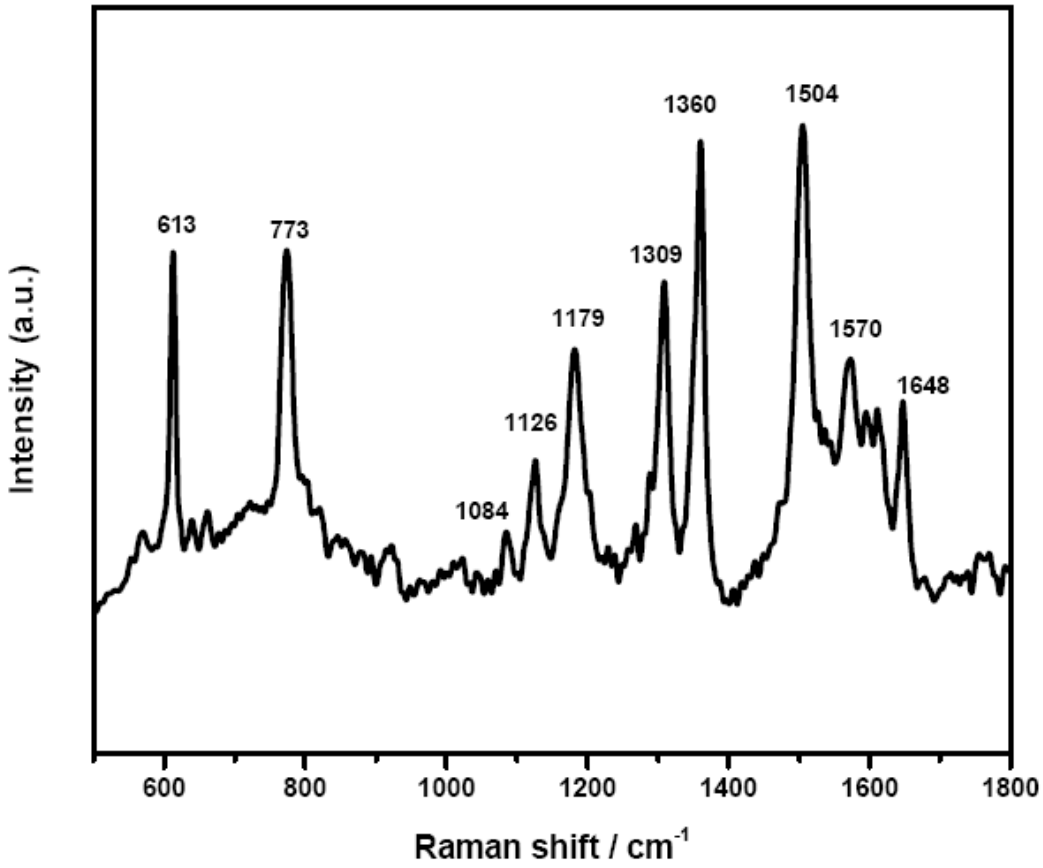

Figure 3.6: SERS spectra of 10^{-5} M Rhodamine 6G with Ag@SiO_2@Au nanoparticles.

3.2.3 Conclusions

Ag@SiO_2@Au core shell metal nanostructures with dielectric silica in between were successfully prepared. These nanostructures have been shown to give SERS of rhodamine

6G. The nanostructure size and dielectric thickness can be further optimized to get better SERS signal and good enhancement factor so that they can be used for ultra trace detection of molecules.

3.3 Effect of capping agent on metal nanoparticles synthesis

3.3.1 Introduction

Metal nanoparticles synthesis requires three starting materials: metal precursor, reducing agent that reduces the metal precursor to metal and capping agent that caps the nanoparticles formed to prevent the aggregation and hence increase stability. Sometimes, capping agent also plays the role of reducing agent. So, here what are the determining factors that govern particle size? Is it reducing agent concentration or volume ratio of reducing to capping agent or is it their chemical nature. In fact, all these factors play important role in the synthesis of nanoparticles. In addition to this, temperature, solvent, surfactant also play important role. One can get nanoparticles of different shapes, sizes and morphologies by varying each of these parameters. Depending on their use, we need to choose reagents that should be used for synthesis. The main motive behind synthesis of different nanoparticles that we are dealing with in this chapter is to get good surface enhanced Raman scattering signal.

So here we are looking at how capping agent determines properties of nanoparticles and further, its implication on SERS. Since the main application of these nanoparticles is in SERS, hence we have shown how SERS changes with the change in properties of silver nanoparticles. Three different silver nanoparticles were used for this study. First synthesis involves nanoparticles formed by citrate reduction of silver as given by Lee et al [29]. Trisodium citrate is a small molecule which acts both as reducing agent and capping agent. In second method, polyvinyl pyrrolidone (PVP), a polymer, capped nanoparticles were synthesized and here too PVP does both the jobs. The third nanoparticles were synthesized by using a strong reducing agent sodium borohydride. No other capping agent was used here.

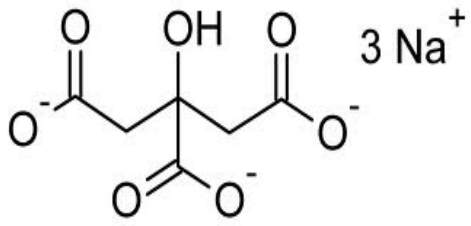

A) Trisodium citrate

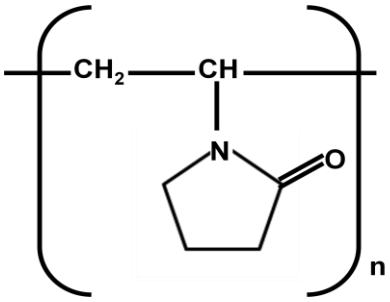

B) Polyvinyl pyrrolidone, PVP

3.3.2 Experimental Details

Chemicals: Silver nitrate and sodium citrate was purchased from Sigma, sodium borohydride was purchased from Merck, PVP was purchased from Loba Chemie and

absolute ethanol was purchased from Commercial Alcohols. For all the synthesis, milli Q water was used.

Preparation of citrate capped nanoparticles: Citrate capped nanoparticles were synthesized by adopting the method given by Lee et al. [29]. Briefly, 18 mg of silver nitrate was added to 100 ml milli Q water and brought to boiling. Then, 2 ml of 1% sodium citrate was added and further boiled for 1 hr.

Preparation of PVP capped nanoparticles: PVP capped silver nanoparticles were prepared by the method given by Chaorong Li et al [23]. Briefly, 100 ml of absolute ethanol and 50 ml of milli Q water was vigorously stirred at 75^{o} C. To this, 10 ml of 0.05 M aqueous solution of silver nitrate was added and stirred for 5 min and heating was continued. Then 20 ml of 2.5 mM PVP was added in aliquots of 1 ml in 5 min. After the mixture was stirred for 20 min at 80^{o} C, 5 ml of 0.1 M NaOH was added to it. The solution was cooled while stirring was continued for 2 hrs after which silver nanoparticles were obtained.

Preparation of silver nanoparticles by borohydride reduction method: This synthesis was done by the method given by Jun Hu et al [30]. Briefly, 100 ml of 5 mM silver nitrate was added drop wise to vigorously stirred and chilled 300 ml, 6mM solution of sodium borohydride. This solution was kept at 40-50^{o} C for 20 min. Then the colloidal

solution was diluted with milli Q water to make a final volume of 500 ml. Change in color of solution to grayish indicates the formation of silver nanoparticles.

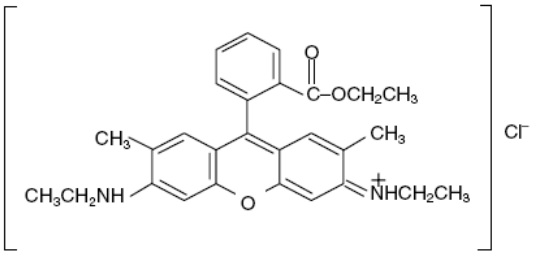

A) Rhodamine 6G (R6G)

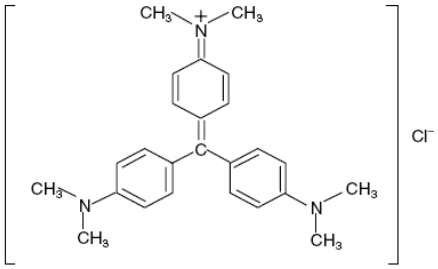

B) Crystal voilet (CV)

Characterization: UV-Vis measurements were done using Perkin-Elmer Lambda 900 UV / Vis / NIR spectrometer. Mie scattering plot was used to calculate particle size. SERS measurements were performed by a custom-built Raman microscope. In the present experiment only red laser with 63nm wavelength was used with laser power of around 10 mW.

3.3.3 Results and Discussions

Silver nanoparticles with different capping agent was synthesized and characterized by UV-Vis measurements. Figure 3.7 shows the extinction spectrum of nanoparticles with different capping agents. It is clear from the graphs that the PVP capped particles are monodisperse with particle size 32 nm. The size distribution is huge when there is no capping agent as the peak is very broad giving average particle size of 30 nm. Broad peak

signifies heterodispersity in particle size. For citrate capped nanoparticles, the particles are more or less monodisperse with mean size of 26 nm as calculated by Mie scattering plot. Scheme 1 shows the silver nanoparticles protected by different capping agents.

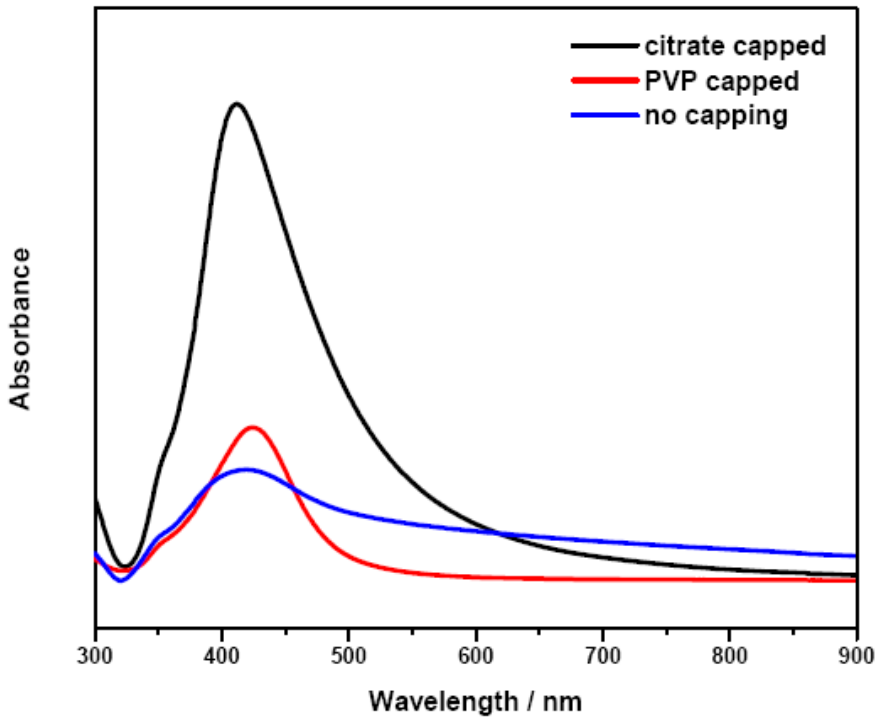

Figure 3.7: Extinction spectrum of silver nanoparticles prepared with citrate capped, PVP capped and no capping.

The synthesized nanoparticles were used as SERS substrate. To look at the activity of these nanoparticles, Crystal Voilet (CV) and Rhodamine 6G (R6G) were chosen as test molecules, as they are known to give good Raman as well as SERS signal. The accumulation time was 10 sec. The graphs were smoothed and baseline corrected. The

molecule to nanoparticle ratio was 1:10 (v/v). Figure 3.8 shows the SERS signal of 10^{-5} M R6G with different silver nanoparticles. It can be seen from the graph that both citrate

Scheme 1:

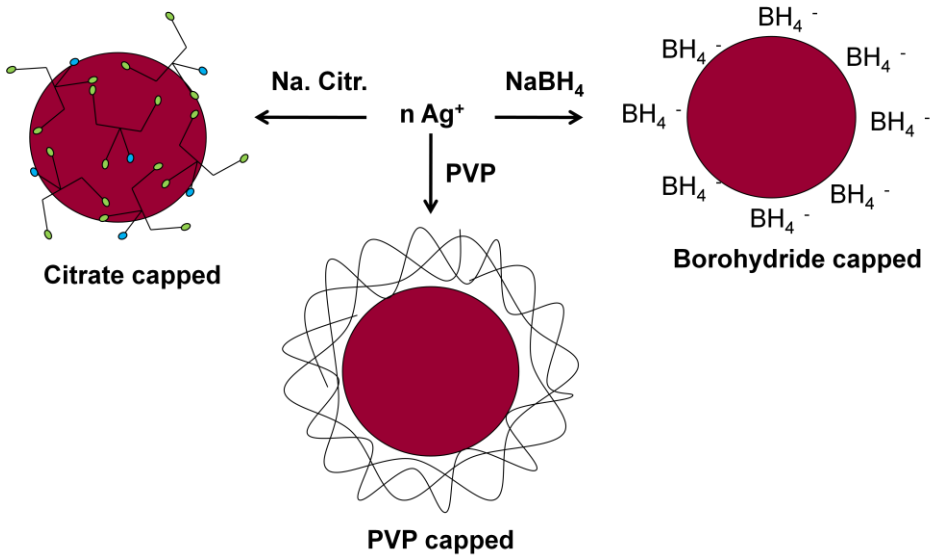

reduced and borohydride reduced silver nanoparticles gave characteristic SERS spectra of R6G. The peak at 1360, 1504, 1570, 1648 cm^{-1} can be assigned to aromatic C-C stretching frequency, a weak peak at 1269 cm^{-1} is due to C-O-C stretch, 1126 cm^{-1} peak can be assigned to C-H in plane bend and C-C stretching frequency. It can be seen that the spectra with PVP capped nanoparticles is completely different. This is because PVP, being a polymer forms a thick shell like coverage over the silver and prevents any other molecule from coming in the close vicinity of the silver core. Thus the signal obtained is of PVP itself. This was also clear when we took the spectra of PVP capped nanoparticles

only. We found that the spectra exactly matched with the above spectra. Similar results were obtained with crystal violet (CV). Figure 3.9 shows the spectra of CV with differently capped nanoparticles. Citrate capped and borohydride capped nanoparticles gave characteristic spectra of CV while PVP capped particle didn't, which was in consistent with the above obtained results. So, for SERS, nanoparticles capped with small molecules should be preferred. Polymer capped nanoparticles must be avoided but if it desired by some specific system then lower concentration of smaller molecular weight polymer should be used.

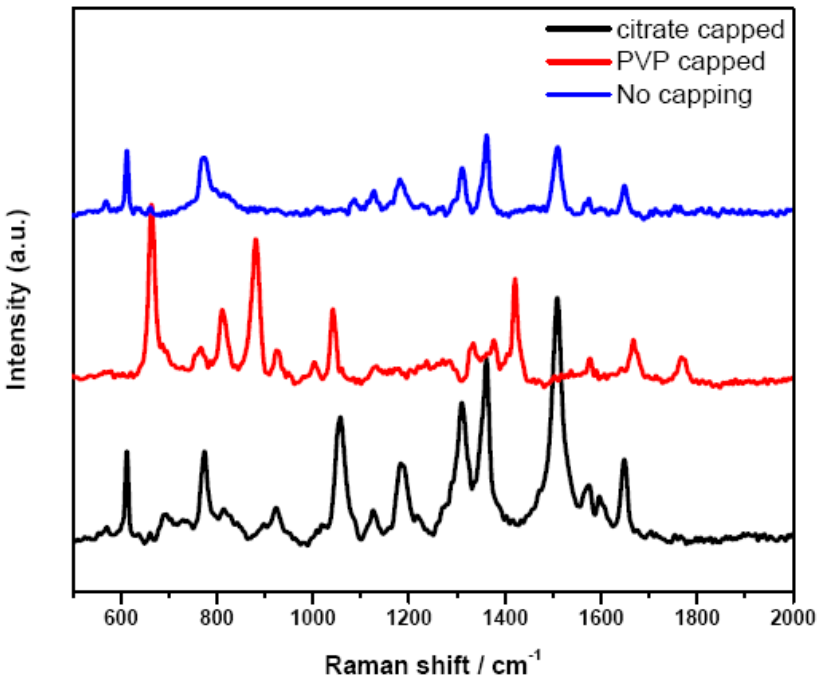

Figure 3.8: SERS spectra of R6G with silver having different capping agents.

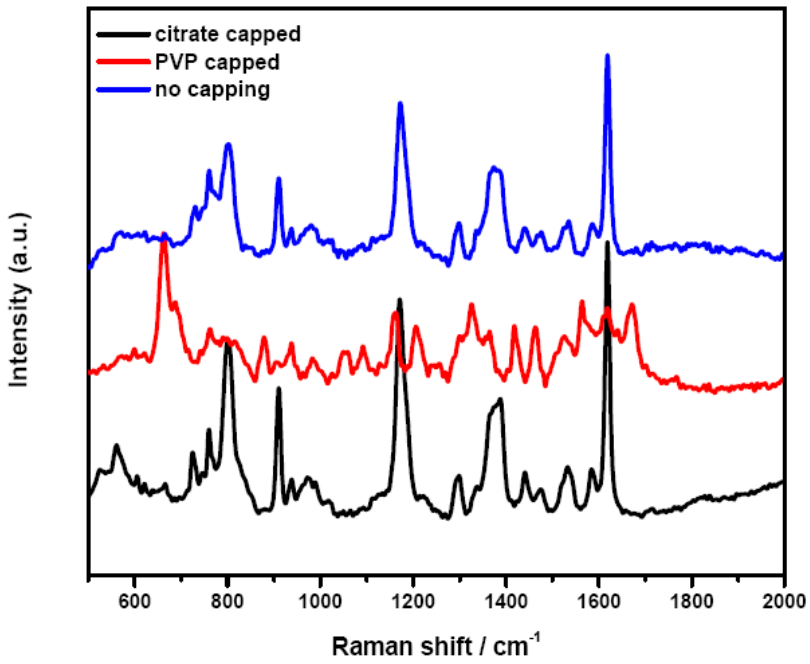

Figure 3.9: SERS spectra of CV with silver nanoparticles having different capping agents.

3.4 Conclusions

Silver nanoparticles with three different types of capping molecules were synthesized. The capping agents were chosen such that the difference between their sizes is high. The use of different capping agents on nanoparticles has been shown to change its properties like size, stability, charge, monodispersity etc. Here we have shown that silver nanoparticles capped with sodium citrate is best for SERS, whereas PVP capped nanoparticles are good for silica coating (discussed previously) but not good as SERS substrate. Silver nanoparticles formed by borohydride reduction are also good for SERS but non-uniformity in size is an issue that must be looked into detail.

3.5 References

1. Caruso, F.; Spasova, M.; Maceira, V. S.; Liz-Marzan, L. M. *Adv. Mater*., **2001**, *13*, 1090.
2. Gittins, D. I.; Susha, A.S.; Schoeler, B.; Caruso, F. *Adv. Mater*., **2002**, *14*, 2508.
3. Pham, T.; Jackson, J. B.; Halas, N. J.; Lee, T. R. *Langmuir,* **2002**, *18*, 4915.
4. Oldenburg, S. J.; Jackson, J. B.; Westcott, S. L.; Halas, N. J. *Appl. Phys. Lett*., **1999**, *75*, 2897.
5. Bohren, C. F.; Huffman, D. R. *Absorption and Scattering of Light by Small Particles*, Wiley, New York, **1983**.
6. Kreibig, U.; Genzel, L. *Surf. Sci.*, **1985**, *156*, 678.
7. (*a*) Sarkar, D.; Halas, N. J. *Phys. Rev. E*, **1997**, *56*, 1102; (*b*) Yu, Y. Y.; Chang, S. S.; Lee, C. L.; Wang, C. R. C. *J. Phys. Chem. B*, **1997**, *101*, 6661.
8. Novak, J. P.; Feldheim, D. L. *J. Am. Chem. Soc.*, **2000**, *122*, 3979.
9. Sun, Y.; Xia, Y. *Anal. Chem.*, **2002**, *74*, 5297.
10. (*a*) Haynes, C. L.; Van Duyne, R. P. *J. Phys. Chem. B*, **2001**, *105*, 5599; (*b*) Underwood, S.; Mulvaney, P. *Langmuir*, **1994**, *10*, 3427.
11. Sun, Y.; Xia, Y. *Analyst*, **2003**, *128*, 686.
12. (*a*) Hermanson, K. D.; Lumsdon, S. O.; Williams, J. P.; Kaler, E. W.; Velev, O.D. *Science*, **2001**, *294*, 1082; (*b*) Chen, S.; Yang, Y. *J. Am. Chem. Soc.*, **2002**, *124*, 5280.
13. (*a*) Knoll, B.; Kellmann, F. *Nature*, **1999**, *399*, 134; (*b*) Sanchez, E. Z.; Novonty, L.;

Xie, X. S. *Phys. Rev. Lett.*, **1999**, *82*, 4014.

14. (*a*) Vo-Dinh, T. *Trends Anal. Chem.*, **1998**, *17*, 557; (*b*) Tessier, P. M.; Velev, O.D.; Kalambur, A. T.; Rabolt, J. F.; Lenhoff, A. M.; Kaler, E. W. *J. Am. Chem. Soc.*, **2000**, *122*, 9554; (*c*) Nie, S.; Emory, S. R. *Science*, **1997**, *275*, 1102; (*d*) Dick, L. A.; McFarland, A. D.; Haynes, C. L.; Van Duyne, R.P. *J. Phys. Chem. B,* **2002**, *106*, 853.
15. (*a*) Sokolov, K.; Chumanov, G.; Cotton, T. M. *Anal. Chem.*, **1998**, *70*, 3898; (*b*) Das, P.; Metiu, H. *J. Phys. Chem.*, **1985**, *89*, 4680.
16. (*a*) Storhoff, J. J.; Elghanian, R.; Mucic, R. C.; Mirkin, C. A.; Letsinger, R. L. *J. Am. Chem. Soc.*, **1998**, *120*, 1959.
17. Liz-Marzan, L. M.; Giersig, M.; Mulvaney, P. *Langmuir*, **1996**, *12*, 4329.
18. Ung T.; Liz-Marzan, L. M.; Mulvaney, P. *J. Phys. Chem. B*, **1999**, *103*, 6770.
19. Lu, Y.; Yin, Y. D.; Mayers, B. T.; Xia, Y. N. *Nano Lett.,* **2002**, *2*,183.
20. Stober, W.; Fink, A.; Bohn, E. *J. Colloid Interface Sci.*, **1968**, *26*, 62.
21. Wang, Z. X.; Chen, X. B.; Chen, M.; Wu, L. M. *Langmuir,* **2009**, *25*, 7646.
22. Shoute, L. C. T.; Bergren, A. J.; Mahmoud, A. M.; Harris, K. D.; McCreery, R. L. *Applied Spectroscopy*, **2009**, *63*, 133.
23. Li, C.; Mei, J.; Li, S.; Lu, N.; Wang, L.; Chen, B.; Dong, W. *Nanotechnology*, **2010**, *21*, 245602.
24. Graf, C.; Blaaderen, A. V. *Langmuir,* **2002**, *18*, 524.
25. Duff, D. G.; Baiker, A.; Edwards, P. P., *Langmuir*, **1993**, *9*, 2301.

26. Hotta, Y.; Alberius, P. C. A.; Bergstrom, L. *J. Mater. Chem.*, **2003**, *13*, 496.

27. Li, G.; Li, H.; Mo, Y.; Huang, X.; Chen, L.; *Chem. Phys. Lett*., **2000**, *330*, 249.

28. Hildebrandt, P.; Stockburger, M. *J. Phys. Chem.*, **1984**, *88*, 5935.

29. Lee, P. C.; Meisel, D. *J. Phys. Chem.*, **1982**, *86*, 3391-3395.

30. Hu, J.; Sheng, R. S.; Xu, Z. S.; Zeng, Y. *Spectrochimica Acta A: Mol. and Biomol. spectrosc.*, **1995**, *51*, 6, 1087.

Chapter 4

Nucleic acid capture and detection by SERRS

4.1 Introduction

There has been immense progress in the area of DNA detection in the last two decades with the increase in interest in DNA based sensing. The growing interest in the field is driven by its large application in DNA diagnostics, gene analysis, fast detection of biological warfare agents, forensic research etc [1-4]. The efficient separation and detection of DNA has become essential for recent advancements in biomedical and pharmaceutical research. Numerous publications have come up illustrating use of different techniques for DNA detection with increased sensitivity, improved selectivity, and possibility of cheaper and faster diagnostics. PCR based amplification techniques [5] are popularly used due to its sensitivity but high cost, sensitive to contamination and not capable in multiplex detection (simultaneous detection of many targets in a single assay) limits its use. Fluorescent spectroscopy based detection techniques [6] are also largely used but have many drawbacks like susceptibility of molecular fluorophore towards bleaching, broad absorption and emission spectrum and cost limitation. Radioactivity [7,8], chemiluminescence are other widely used techniques in biodetection. One of the

major drawbacks in all these techniques is their inability to detect viral DNA at early stage of disease without using amplification techniques like Polymerase Chain Reaction (PCR), where the concentration of pathogen DNA/RNA in the blood serum is very low. So, we must look into ways in order to overcome these drawbacks hence making disease detection possible at preliminary stage.

Surface Enhanced Raman Scattering (SERS) technique has grown extensively in recent years. Recent advancement in SERS and its ability to detect single molecule has turned it into an extremely sensitive technique for ultra low detection [9]. DNA detection techniques are generally based on hybridisation of target DNA and complementary DNA either in solution or on solid support. The solid support can either be planar glass substrate or nanoparticles that have been functionalised with complementary DNA strand. DNA biosensors and DNA microarrays are also being used largely. Recently nanoparticles based detection techniques are explored immensely due to various advantages like ease of synthesis of nanoparticles, size and shape dependent absorption properties, robustness etc. Nanoparticle surface can easily be modified or functionalised in order to bind to the target. Different types of nanoparticles can be used for bio detection. The basic criterion is that they should not interfere with the biological system and must be robust enough to withstand different pH environments. Metal nanoparticles, for instance silver and gold colloids are being extensively used for SERS based DNA detection. Silver has the highest enhancement factor amongst metal known so far while gold is biocompatible. The problem with silver is that it is toxic and cannot be used for

in-vivo applications. This problem was overcome by developing core shell nanoparticles having silver core and gold shell [10-12]. The core size and shell thickness can be optimised to get maximum SERS enhancement. Second type of detection method basically involves DNA capture by functionalised superparamagnetic nanoparticles of haematite or magnetite [13]. Using magnetic nanoparticles facilitates easy washing cycle without losing DNA. This increases the sensitivity. Magnetic nanoparticles can be coated with gold or silver. The coating increases the stability of magnetic nanoparticles and also reduces the toxicity. Further since silver or gold nanoparticles support surface plasmon they can be used for DNA detection technique based on SPR and SERS. Magnetic nanoparticles can be coated with silica. The advantage of silica surface is that it can easily be functionalised to bind to amino modified DNA through diisothiocyanate linker molecule. Thus DNA remains completely locked up with the silica surface by strong chemical bonds. Several other combinations of core shell nanoparticles that utilize the advantage of each of them can also be used to serve the necessary purpose.

In this chapter, the synthesis of magnetic core silica shell nanoparticles and the possibility of DNA detection using them through a three way capture and then detection by SERS, has been discussed. The scheme for capture of DNA by nanoparticles and detection has been shown below (scheme 1).

Scheme 1:

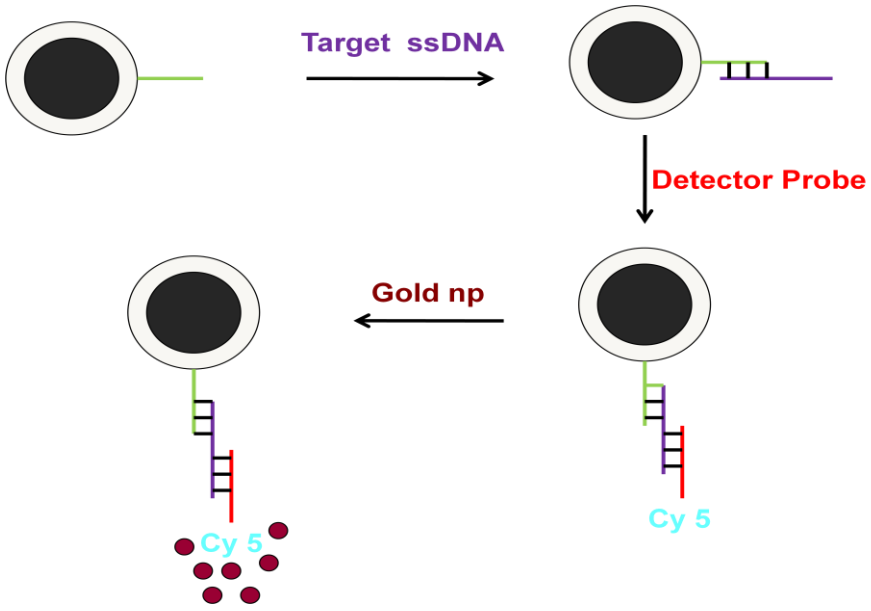

4.2 Experimental Details

Chemicals: Iron(II) chloride, iron(III) chloride, sodium borohydride and 3-aminopropyl triethoxysilane (APTES) and phenylene diisothiocyanate (PDC) were purchased from Sigma-Aldrich; N,N,N,N-cetyl trimethyl ammonium bromide (CTAB) was bought from Himedia; n-butanol was purchased from Loba Chemie; N,N- dimethyl formamide (DMF), dichloromethane (DCM), iso-octane and methanol were bought from Qualigens. Ammonia solution and tetraethyl orthosilicate (TEOS) from Merck; HCl and toluene from s.d.fine-chem Ltd, ethanol from Commercial Alcohols; and pyridine from Rankem were purchased. Milli Q water was used for all the preparations.

Synthesis of Fe_3O_4 nanoparticles: Magnetic nanoparticles were prepared by the adopting the method given by Lin et al [14]. Briefly, in test tube A, 0.1294g of $FeCl_3.6H_2O$, 0.0472g of $FeCl_2.4H_2O$, 0.6g of CTAB, 0.6174 ml of butanol and 2.19 ml of octane were added and mixed by sonication for 10 min. Then 0.474 ml of water was also added to maintain the molar ratio of water to CTAB equal to 8. In test tube B, 0.1021g of $NaBH_4$, 0.6g of CTAB, 0.6174 ml of butanol and 2.19 ml of octane were added and sonicated for 10 min. Contents of both the test tubes were simultaneously poured in a beaker and stirred with mechanical stirrer at 60 ^oC for 20 min. Magnetic nanoparticles formed were washed four times in water and four times in methanol.

Scheme 2:

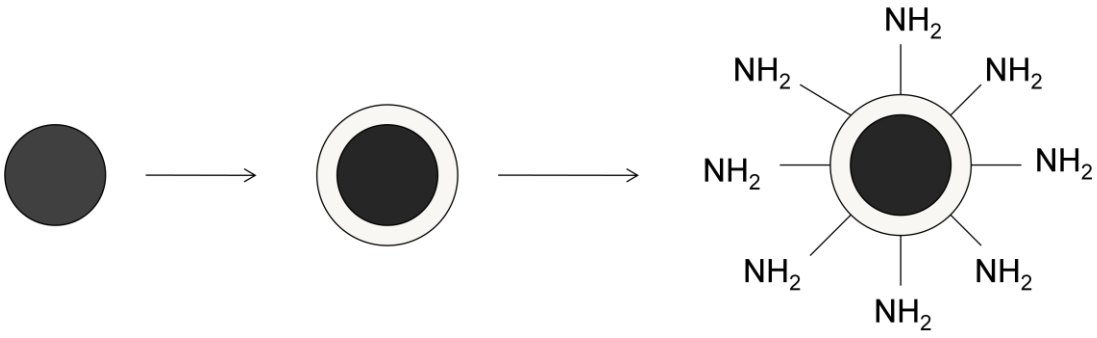

Silica coating: For silica coating, modified Stober process [15] as given by Shao et al [16] was used. Briefly, 10mg of above prepared magnetic nanoparticles were treated with 10 mL of 2 M solution of HCl under ultrasonic vibration for 5 min. This was then thoroughly washed with milli Q water and redispersed in a mixture containing 40 ml of

ethanol, 10 ml milli Q water and 2 ml of 25 wt% ammonia solution. The mixture was sonicated for 10 min. Then, aliquots of TEOS (10,20,40,80,160, 200µL) was added at fixed intervals and the reaction was allowed to proceed for 1 hr. Silica coated magnetic nanoparticles were separated with magnet and washed in a 1:1 v/v mixture of ethanol and water, dried and kept for further use. Scheme 2 and 3 show the different steps involved in the process.

Scheme 3:

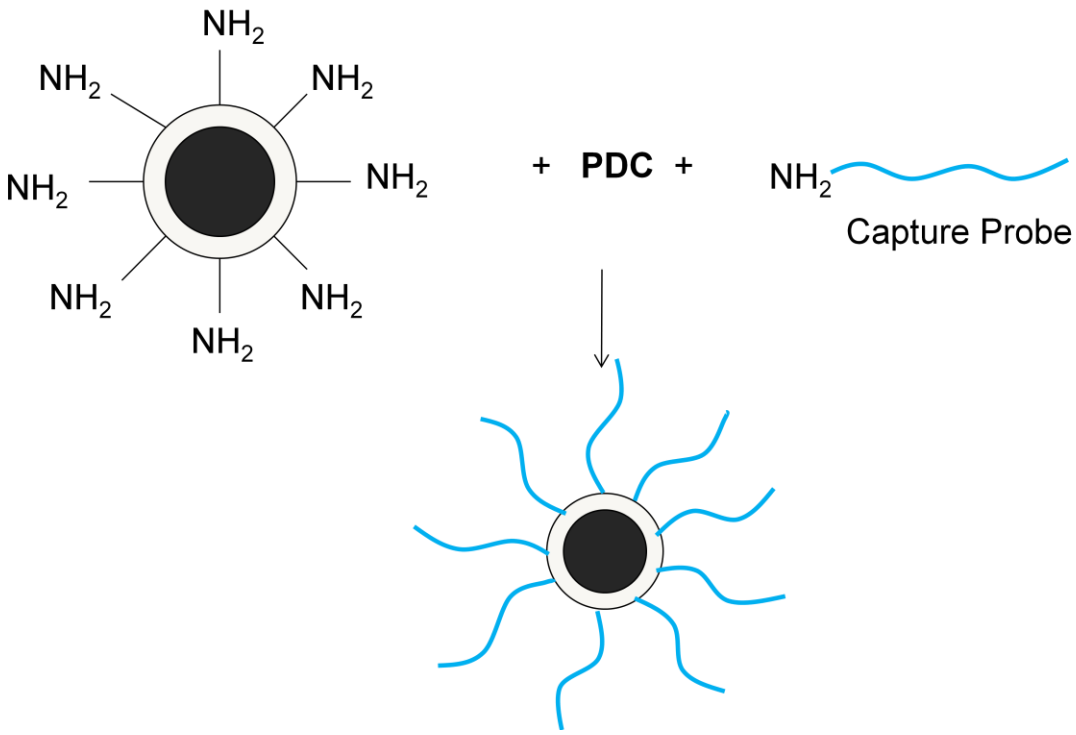

Functionalisation of silica surface: Magnetic core silica shell nanoparticles were cleaned by rinsing in 2ml of 6 M HCl solution with gentle shaking at room temperature for 12 hrs. They were then extensively washed with water until the pH becomes neutral. The nanoparticles were then baked in oven at 110 ^{o}C for 2½ hrs. The cleaned nanoparticles (30mg) were dispersed in 5 ml of 2% solution of APTES in anhydrous toluene, sonicated for 10 min and shaken for 10 hrs. Then it was washed with dry toluene (in argon atmosphere) four times and dried. Silanised nanoparticles were derivatised with phenylene diisothiocyanate solution. Briefly, silanised particles were rinsed in 2 ml solution of DMF containing 10% pyridine and 0.2% phenylene diisthiocyanate and shook for 2 hrs at room temperature. The nanoparticles were then washed five times with DMF, three times with absolute ethanol and three times with methylene chloride, dried and kept for further use.

The oligonucleotides sequences used are as following:

1. Target:

5′CCCATTAACATTTGGATGGTGCTGTCCGTCTGTTGTGTGACTCTGGTAACT 3′

2. Capture Probe:

NH_2- 5 ′AGCACCATCCAAATGTTAATGGG 3′

3. Detector probe:

Cy5-5′ AGTTACCAGAGTCACACAACAGACGG 3′-NH_2

Characterizations

The magnetic core silica shell nanoparticles were characterised by TEM and UV-Vis measurements. The charge on particles was found by Zeta potential measurements. SERS spectra were recorded with 633nm He-Ne laser.

4.3 Results and Discussions

Figure 4.1 shows the TEM image of magnetic core silica shell nanoparticles. We can see that the coating took place on a cluster of particles giving a total particle size of about 500 nm. Here the large particle size is not a problem because their only role is to capture the oligonucleotides thus making the washing cycle easier through magnetic separation.

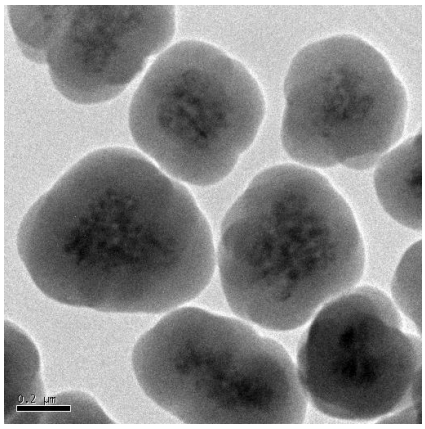

Figure 4.1: TEM image of Fe_3O_4@SiO_2 nanoparticles.

Figure 4.2 and 4.3 show the extinction spectra of Fe_3O_4 and Fe_3O_4@SiO_2 nanoparticles respectively. It can be seen that the absorption peak of bare magnetic nanoparticles is

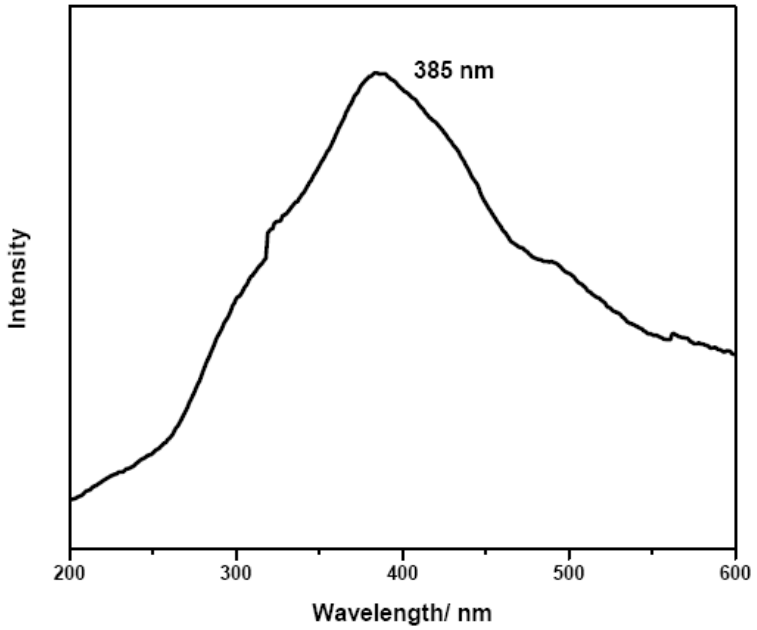

Figure 4.2: Extinction spectrum of Fe_3O_4 nanoparticles.

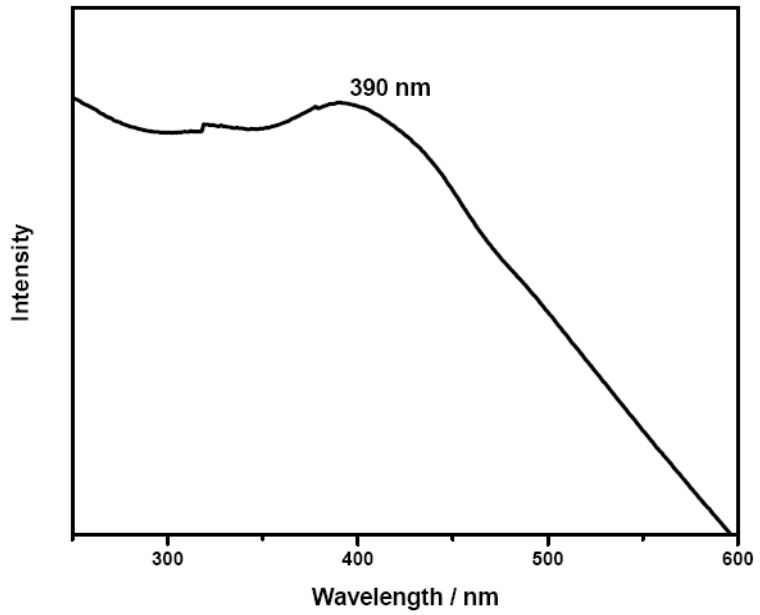

Figure 4.3: Extinction spectrum of Fe_3O_4@SiO_2 nanoparticles.

around 385 nm and the particles are predominantly monodisperse with the mean size around 8 nm. The silica coating further broadens the absorbance peak by absorbing most of the light passing through it, and the adsorption peak shifts to 390 nm. The particles were superparamagnetic in nature. After magnetically separating them from the solution, they get redispersed again with slight shaking.

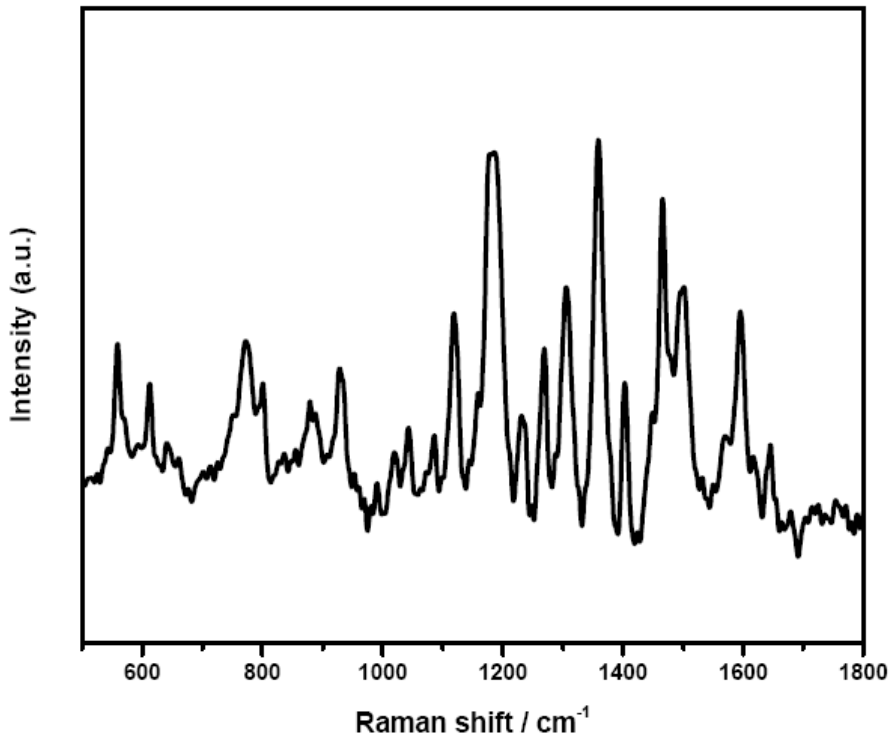

Figure 4.4: SERS spectra of 10^{-7} M Cy5 tagged oligonucleotide with gold nanoparticles.

SERS spectra of Cy 5 tagged oligonucleotide with gold nanoparticles were recorded and shown in figure 4.4. The spectra show characteristic peaks of Cy 5 as reported in the

earlier literatures [2]. The accumulation time was 10 sec, recorded with He-Ne laser (633nm). λ_{max} for Cy 5 is around 640 nm.

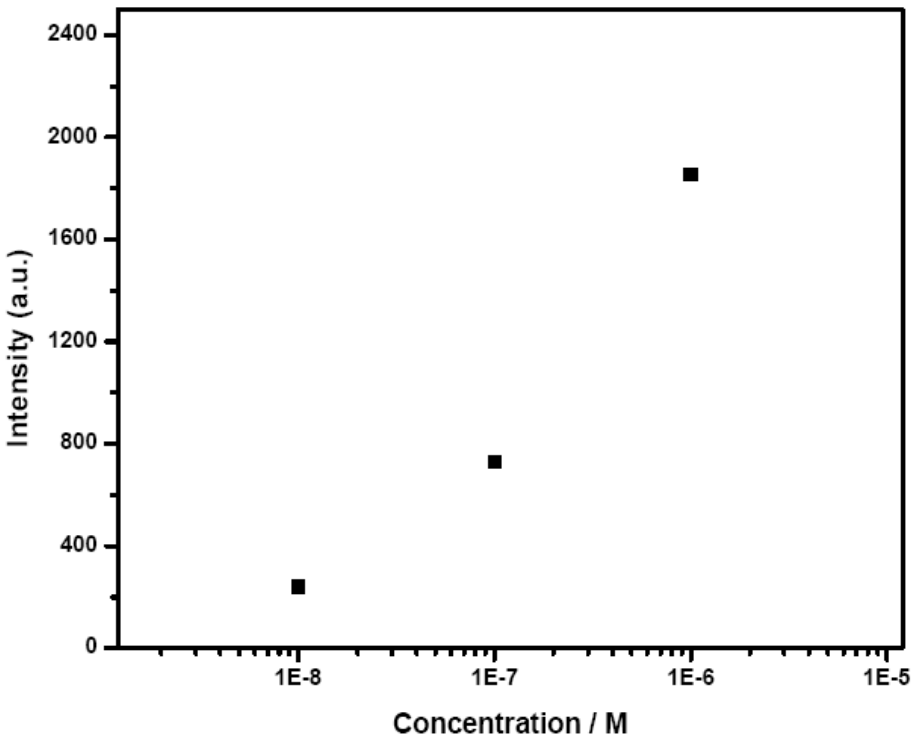

Figure 4.5: Intensity vs concentration plot for 1125 nm peak observed in oligo tagged Cy 5.

SERS spectra at three different concentrations i.e. 10^{-6}, 10^{-7}, 10^{-8} M Cy5 tagged oligonucleotides were recorded. Change in intensity of 1125 nm peak plotted as change in concentration has been shown in figure 4.5. It was observed that there is an exponential decrease in intensity with decrease in concentration of oligos. For 10^{-9} M

concentration peaks with very less intensity were observed. Currently, we are working on introducing looped structures and charge repulsion species to increase the Signal to Noise Ratio and the sensitivity.

4.4 Conclusions

Magnetic core silica shell nanoparticles were synthesized and characterised. The nanoparticles were superparamagnetic in nature. The silica shell was chemically modified by APTES in order to bind to amino group at the 3′ end of the oligonucleotide through the linker molecule phenylene diisothiocyanate. It was noted that mass of magnetic nanoparticles before and after 10 wash cycles were same, thus there is no loss of nanoparticles during washing. Hence DNA bound to the nanoparticles cannot be lost during the wash cycles. SERS spectra of oligonucleotide modified with Cy 5 were shown at different concentrations of oligonucletide. We could obtain signal till 10^{-9} M concentration of oligonucletotide but the signal strength was very weak. The signal intensity was shown to fall exponentially with decrease in concentration.

Future Scope

These nanoparticles can be used for DNA extraction and detection by SERS. One of the major challenges in bio-diagnostics is the loss of analyte during the wash cycles. DNA detection by capturing it with silica coated magnetic nanoparticles is probable way of extracting DNA, further preventing its loss during washing cycles. Charge, steric

repulsion etc are few other deciding factors that either prevent or aid binding. These conditions once optimized would develop this technique into a potential and highly reliable technique for DNA detection.

4.5 References

1. Xiang, C. C.; Chen, Y. *Biotechnol. AdV.,* **2000**, *18*, 35.
2. Cao, Y. W. C.; Jin, J.; Mirkin, C. A.; *Science*, **2002**, *297*, 1536.
3. Isola, N. R.; Stokes, D. L.; Vo-Dinh, T. *Anal. Chem.* **1998**, *70*, 1352.
4. Rhodes, D. R.; Chinnaiyan, A. M. *J. Invest. Surg.*, **2002**, *15*, 275.
5. Saiki, R. K.; Scharf, S.; Faloona, F.; Mullis, K. B.; Horn, G. T.; Erlich, H. A.; Arnheim, N. *Science*, **1985**, *230*, 4732, 1350.
6. Qiu, B.; Zheng, Z. Z.; Lu, Y. J.; Lin, Z. Y.; Wong, K.Y.; Chen, G. N.; *Chem. Comm.*, **2011**, *47*, 1437.
7. Livache, T.; Roget, A.; Dejean, E.; Barthet, C.; Bidan, G.; Teoule, R., *Nucleic acid Res.*, **1994**, *22*, 2915.
8. Su, H. B.; Kallury, K. M. R.; Thompson, M.; Roach, A. *Anal. Chem.*, **1994**, *66*, 769.
9. Nie, S.; Emory, S. R. *Science*, **1997**, *275*, 1102.
10. Kumar, G. V. P.; Shruthi, S.; Vibha, B.; Reddy, B. A. A.; Kundu, T. K.; Narayana, C. *J. Phys. Chem. C*, **2007**, *111*, 4388.
11. Douglas, F. ; Yanez, R. ; Ros, J.; Marin, S.; Muniz, A. E.; Alegret, S.; Merkoc, A.

J Nanopart Res, **2008**, *10*, 97.

12. Pande, S. et al, *J. Phys. Chem. C,* **2007,** *111*, 10806.
13. Bromberg, L. et al, *Langmuir*, **2010**, 26, *11*, 8829.
14. Lin, J. et al, *Journal of Solid State Chemistry*, **2001**, *159*, 26.
15. Stober, W.; Fink, A.; Bohn, E., *J. Colloid Interface Sci.,* **1968**, *26*, 62.
16. Shao, D. et al *J. of Colloid and Interface Science*, **2009**, *336*, 526.

Future Outlook

Surface Enhanced Raman Scattering is a very versatile technique with a potential to carry out ultra low detection. Different applications of SERS include single molecule detection, simultaneous detection of multiple contaminant present in the sample, Raman or SERS mapping/imaging of cell etc. TERS, a combination of SERS with atomic force microscopy has opened new research possibilities with spatial resolution in nanometer regime. Because of its sensitivity to detect even slight changes in molecular configuration, SERS is used for environmental analysis to find toxicity in ground water and concentration of pollutants in the air. In addition to this, detection of explosive chemicals has also been made possible through SERS. It has an edge over many other traditional techniques like fluorescence and chemiluminescence. The advantages include high sensitivity, multiplex detection, robustness etc. There are still loop holes in the SERS technique that need to be tackled. It is not uncommon to get different spectra within the same sample spot while recording SERS. Trivial changes in the SERS substrate like nanoparticles shape, size, and extent of aggregation, substrate surface chemistry, analyte orientation or analysis conditions can manipulate SERS spectra. Sometimes, we also see unstable SERS spectra produced when signals from SERS hotspots govern the spectra or when longer exposure to laser light degrades the analyte or SERS substrate. To circumvent above problems, few modifications in recording SERS spectra have been done like use of low laser power. Further, use of micro fluidic cells that

create turbulent flow conditions which causes the mixing of analyte, activator and colloid and also allows an average measurement to be taken is advantageous in many respects. In order to minimize the effect of fluctuations in SERS substrate, isotopically labeled internal standards have also been used.

Despite many hurdles, SERS is rapidly growing into practical tool for detection. Its applications are not only confined to laboratory research but applications like microfluidic cells, lab on chip method with portable Raman systems have facilitated qualitative and quantitative field analysis. Thus, SERS has great potential to be used as an analysis tool.